Diplomarbeit

Towards iron nanoparticle-based stem cell imaging *in vivo*

eingereicht von

Daniel Liebmann (geb. Gungl)
23. 02.1986

zur Erlangung des akademischen Grades

Doktor der gesamten Heilkunde
(Dr. med. univ.)

an der

Medizinischen Universität Graz

ausgeführt an der

Stem Cell Research Unit (SCRU)
Klinischen Abteilung für Hämatologie,
Universitätsklinik für Innere Medizin,

unter der Anleitung von

Univ.-Prof. Dr. Dirk Strunk

und

Dr. Andreas Reinisch, PhD

Graz, 20. Februar 2014

Sehet im Studium nie eine Pflicht,
sondern die beneidenswerte Gelegenheit die befreiende
Schönheit auf dem Gebiet des Geistes kennenzulernen.
Zu eurer eigenen Freude und zugunsten der Gemeinschaft der
euer späteres Wirken gehört.

(Albert Einstein)

Table of Contents

Eidesstattliche Erklärung

Ich erkläre ehrenwörtlich, dass ich die vorliegende Arbeit selbstständig und ohne fremde Hilfe verfasst habe, andere als die angegebenen Quellen nicht verwendet habe und die den benutzten Quellen wörtlich oder inhaltlich entnommenen Stellen als solche kenntlich gemacht habe.

Graz, am 20. Februar 2014

Danksagung

Ich möchte mich an dieser Stelle bei allen Personen der SCRU für die freundliche Aufnahme und die große Hilfsbereitschaft bedanken. Ein großes Dankeschön ergeht an Dirk Strunk, der mir die Gelegenheit gegeben hat einen Einblick in die faszinierende Welt der Forschung zu erlangen und diese Arbeit vornehmlich betreut hat. Ebenso zu danken habe ich Andreas Reinisch für die unermüdliche Hilfe, Diskussion und Unterstützung im Rahmen der Laborarbeit sowie Clemens Diwoky für die nicht enden wollende Geduld bei Fragen zur MRT. Auch allen anderen Mitgliedern, Anna, Nici, Daniela, Birgit, Eva, Katharina, Margaretha und Roksareh, möchte ich meinen Dank aussprechen für die ständige Diskussions- und Hilfsbereitschaft.

Zutiefst dankbar bin ich meinen Eltern, für die stete und bedingungslose Unterstützung die sie mir zukommen ließen, aber vor allem für den liebevollen Blick auf eine, in jedem Detail faszinierende Welt.

Meiner Schwester Anna danke ich für den guten Zuspruch und viele hilfreiche Kommentare.

Schlussendlich danke sagen möchte ich dir, Antonia, für deine endlose Geduld und die liebevolle Unterstützung die du mir zu jeder Tages- und Nachtzeit zuteilwerden lässt und dir, Maximilian, für die große Freude die mir deine Anwesenheit beschert.

Zusammenfassung

In den letzten Jahren sind große Hoffnungen in das Konzept der regenerativen Medizin gesetzt worden. Dieses sieht vor, dass durch das Verabreichen von Stamm- und Vorläuferzellen, mit dem Potential erkranktes Gewebe zu unterstützen oder zu ersetzen, Heilung erreicht werden kann. Daher ist es auch notwendig, Werkzeuge zu entwickeln die eine Untersuchung und Beantwortung wichtiger Fragen, wie die Art der Verabreichung, der Verteilung der Zellen im Körper oder die Feststellung des Engraftments, also des Anwachsens bzw. das Ankommen im Zielorgan, erlauben.

Eine Möglichkeit diese Fragen zu beantworten ist die Benutzung der Magnetresonanztomographie (MRT). Diese bietet Auflösungen bis in den Mikrometerbereich sowie verschiedene Mechanismen um Bildkontrast zu erzielen. Ein weiterer Vorteil ist die Anwendbarkeit sowohl im experimentellen, wie auch im präklinischen Einsatz.

Diese Arbeit untersucht verschiedene Möglichkeiten mesenchymale Stamm- und Vorläuferzellen sowie endotheliale Kolonie-bildende Vorläuferzellen mit Kontrastmitteln für die MRT zu markieren. Verschiedene Zusammensetzungen von Molday Ion™, sehr kleinen superparamagnetischen Eisenoxidpartikeln, und Resovist®, kleinen superparamagnetischen Eisenoxidpartikeln, wurden hinsichtlich ihrer Aufnahme in Zellen untersucht. Resovist® wurde erfolgreich aufgenommen. Es konnte gezeigt werden, dass dadurch keine Einschränkung der Differenzierungsfähigkeit oder der Funktionalität auftritt.

Das Detektionslimit zweier verschiedener MRT-Sequenzen, welche ein hohes Kontrast/Rausch Verhältnis bei niedriger Aufnahmezeit aufweisen, wurde an einem *in vivo* Mausmodell erprobt. Dabei wurde ein MRT Artefakt gefunden, welches durch markierte Zellen mit hoher Eisenbeladung hervorgerufen wird. Eine MRT-Sequenz in Verbindung mit einem Nachbearbeitungsschritt, die auf dieses Artefakt optimiert wurde, erlaubte die Darstellung von einzelnen markierten Zellen. Diese Sequenz bietet daher gute Voraussetzungen für einen weiteren Einsatz in der Verfolgung von markierten Stammzellen.

Abstract

Regenerative medicine is believed to offer a curative treatment for diseases by transplantation of cells with potential to regenerate or support damaged tissue. Therefore, necessary cell tracking tools have to be developed for answering therapeutically important issues like delivery route, cellular distribution pattern or the determination of engraftment.

Magnetic resonance imaging (MRI) provides resolutions in the higher micrometer range, offers different contrast modifying methods even for cells, can be used not only in an experimental but also a preclinical setting and has only few limitations like longer acquisition times or a low specificity.

This thesis examines ways of labeling mesenchymal stem and progenitor cells (MSPCs) and endothelial colony-forming progenitor cells (ECFCs) with contrast agents for MRI. Different formulations of ultrasmall superparamagnetic iron oxide (USPIO) particles, Molday Ion™, and superparamagnetic iron oxide particles (SPIOs), Resovist® were tested for their uptake. Cells were successfully labeled with Resovist® and subsequent assays showed no reduction of adipogenic, osteogenic and chrondogenic differentiation in MSPCs and network formation in ECFCs.

The cellular detection limit of two different MRI sequences providing a high contrast-to-noise ratio in combination with a low acquisition time were studied with an *in vivo* mouse model. It was possible to find an MRI artifact created by cells labeled with high doses of SPIOs. An optimized MRI sequence with a postprocessing step, dedicated to this artifact, permitted the visualization of single cells thus making it an appropriate candidate for further cell tracking applications.

List of Figures

List of Tables

Abbreviations

ATP	Adenosine triphosphate
BLI	Bioluminescence imaging
BM	Bone marrow
BMAC	Bone marrow aspirate container
bSSFP	Balanced steady state free precession sequence
bUTE	Balanced ultrashort time of echo sequence
CAC	Circulating angiogenic cell
CF-4	Four-layered cell factory
CFU	Colony-forming unit
CNR	Contrast to noise ratio
CT	Computed tomography
DAPI	Diamidino phenylindole
DMSO	Dimethyl sulfoxide
DTPA	diethylene triamine pentaacetic acid
ECFC	Endothelial colony-forming progenitor cell
EDTA	Ethylenediaminetetraacetic acid
EPC	Endothelial progenitor cell
FID	Free induction decay
FITC	Fluorescein isothiocyanate
FLASH	Fast low angle shot sequence
FOV	Field of view
GRE	Gradient recalled echo sequence
HPP	High proliferative potential
HSCTx	Hematopoietic stem cell transplantation
IBMX	3-Isobutyl-1-methylxanthine
ISCT	International society for cellular therapy
LE	Late echo
LMP	Low melting point

LPP	Low proliferative potential
MEM	Minimum essential medium
MR	Magnetic resonance
MRI	Magnetic resonance imaging
MSC	Mesenchymal stem cell
MSPC	Mesenchymal stem/progenitor cell
NIR	Near infrared
NM	Net magnetization
PBS	Phosphate buffered saline
PEG	Polyethylen glycol
PET	Positron emission tomography
pHPL	Pooled human platelet lysate
PLL	Poly-L-lysine
POPC	Palmitoyl-oleoyl-phosphatidylcholine
PS	Protamine sulfate
RF	Radiofrequency
RPMI	Roswell Park Memorial Institute
SI	Signal intensity
SNR	Signal to noise ratio
SPE	Spin echo sequence
SPECT	Single-photon emission computed tomography
SPIO	Superparamagnetic iron oxide particle
TE	Time of echo
TGF-β3	Transforming growth factor-β3
TR	Repetition time
UC	Umbilical cord
UCB	Umbilical cord blood
USPIO	Ultrasmall superparamagnetic iron oxide particle
UTE	Ultrashort time of echo sequences

1 Introduction

1.1 Stem Cell Based Therapy

In 1956 Barnes et al. demonstrated the successful treatment of leukemia by sublethal irradiation followed by infusion of normal bone marrow (BM) in mice (Barnes et al., 1956). The treatment of human patients was reported at the same time and it was up to Thomas et al. who first successfully transplanted marrow cells after irradiation in 1956 (Thomas, 1999). Fifty-five Years later, more than 20 000 human transplantations of hematopoietic cells from marrow, peripheral blood or cord blood are being performed annually. Many disciplines have been involved in the research of this growing field, including radiation biology, immunology, molecular biology, drug development, blood component transfusion technology and numerous clinical disciplines.

Although the term stem cell based therapy is often used as a synonym for hematopoietic stem cell therapy it also includes the use of non-hematopoietic stem cells for therapeutic purposes. The identification and better characterization of these cells has been fundamental to the development of the concept of regenerative medicine. Regenerative medicine makes use of cells which are capable of maintaining the stromal and vascular microenvironment and regeneration of tissue. Two important cell types are mesenchymal stem/progenitor cells (MSPCs) and endothelial colony-forming progenitor cells (ECFCs).

Many questions still have to be answered to establish stem cell transplantation as therapy of choice for diseases other than leukemia and lymphoma or myeloma. Questions unresolved include that of the optimal tissue source for a specific therapeutic setting as well as the therapeutically important issues of delivery route, cellular distribution pattern or the determination of engraftment.

1.2 Adult Stem Cells

Adult stem cells, also known as somatic stem cells, are present in fetal as well as in adult human and animal bodies after adolescence. Their designated application and use in regenerative medicine is a result of the ability to self-renew during cell division and their hypothetic multipotentiality.

1.2.1 Mesenchymal Stem/Progenitor Cells (MSPCs)

First studies by Friedenstein and colleagues reported the presence of fibroblastoid marrow cells in the 1970s and their clonogenic potential. The German pathologist Cohnheim had already proposed that bone marrow can be the source of fibroblasts contributing to wound healing in numerous peripheral tissues about 100 years earlier (Schepina and Henry M. Kronenberg, 2009; Prockop, 2007). Further experiments on these fibroblast-like cells revealed remarkable cell functions and led to the term mesenchymal stem cells (MSC) even though the term multipotent stromal cell has been proposed as a better replacement due to the lack of experimental proof of 'stemness', but still remains controversial (Bianco, 2011; Bianco et al.., 2008).

Since MSPCs were first identified in human bone marrow, they have also been isolated from virtually all tissues including adipose tissue (AT), umbilical cord blood (UCB), peripheral blood (PB), synovial membrane, placenta, and amniotic fluid.

The great diversity of MSPC-containing tissue and MSPC production methods potentially leads to a great heterogeneity in the resulting cell population despite their morphological similarity. The International Society for Cellular Therapy (ISCT) position statement defined minimal criteria for defining multipotent mesenchymal stromal cells illustrated in Figure 1. First, MSPC must be plastic-adherent. Second, MSPC must express CD73 (ribonucleotide phosphohydrolase), CD90 (thymus cell antigen-1) and CD105 (endoglin) at an extent of > 90%, and lack expression of CD45 (common leukocyte antigen), CD34 (hematopoietic stem cell marker), CD14 (lipopolysaccharide-receptor) or CD11b (complement receptor [CR3] subunit), CD79α (immunoglobuline α) or CD19 (B-cell co-receptor subunit) and HLA-DR (MHC cell surface receptor) surface molecules (< 5%). Third, MSPC must differentiate to osteoblasts, adipocytes

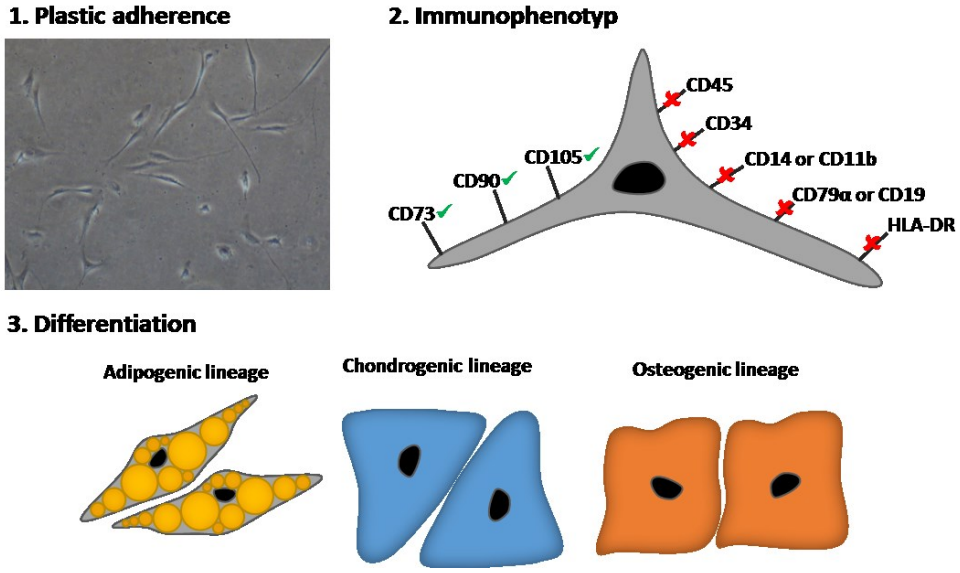

Figure 1: The three minimal requirements for defining a multipotent mesenchymal stromal cell as defined by the International Society for Cellular Therapy (ISCT).

and chondroblasts *in vitro* (Dominici et al., 2006). It is a matter of debate whether these three lineages of differentiation already confirm multipotentiality.

It has turned out, that MSPCs provide a broad range of capabilities and therefore have emerged as a promising tool for clinical application. MSPCs carry different immunomodulatory properties like the prevention of allorecognition, establishment of a vicinal immunosuppressive microenvironment or interference with dendritic cell and T-cell function. Immune modulatory properties of MSPCs *in vivo* and *in vitro* have been reviewed in detail (Nauta and Fibbe, 2007). The therapeutic application of immunosuppressive properties of MSPCs has already been utilized for the treatment of acute graft-versus-host-disease (GVHD) after allogeneic stem cell transplantation (Le Blanc et al., 2004; Ringdén et al., 2006).

MSPCs are major components of the hematopoietic stem cell niche known to be involved in the regulation of hematopoietic stem cell (HSC) maintenance and proliferation. Based on animal studies in which co-transplantation of MSPCs with HSCs improved engraftment of the latter, MSPCs have been exploited for their ability to improve HSC engraftment (Battiwalla and Hematti, 2009)

Furthermore MSPCs have emerged as a promising therapeutic tool for tissue regeneration and repair. Due to their initial source, MSPCs were originally evaluated for their capacity to repair skeletal defects in human patients suffering from osteogenesis imperfecta (Horwitz et al., 2001; Otsuru et al., 2012). MSPCs were also

tested in animal models of lung injury, kidney disease, diabetes, myocardial infarction and various neurological disorders (Phinney and Prockop, 2007)

1.2.2 Endothelial Colony-Forming Progenitor Cells (ECFC)

Angiogenesis describes the process of vascular remodeling and regeneration through proliferation and subsequent migration of mature endothelial cells from pre-existing vessels. It was the predominant concept for adult vascular regeneration until the work of Asahara and Colleagues. They described endothelial progenitor cells (EPCs), a circulating cell type within a CD34+ enriched population of mononuclear blood cells with endothelial phenotype and function contributing to neovascularization (Asahara et al., 1997). These putative EPCs were termed colony-forming units (CFU) of EPCs (later on CFU-Hill), but were redefined after clonal analysis showing their hematopoietic origin (Rohde et al., 2006; Yoder et al., 2007). Although these cells lack a true endothelial progenitor phenotype they appear to have pro-angiogenic activity (Hirschi et al., 2008).

A major step towards identification of a true endothelial progenitor cell population was the identification of an entire hierarchy of endothelial colony-forming cells (ECFCs) in human blood consisting of low proliferative potential (LPP-) ECFCs and high proliferative potential (HPP-) ECFCs (Ingram, 2004). Due to their late appearance in culture (after 2-4 weeks) compared to CFU-Hill and other circulating angiogenic cells (CACs), ECFC have also been called “late outgrowth EPCs”, whereas CFU-Hill and CAC that appear after 3-4 days of culture have been termed “early outgrowth EPCs”. Unlike CFU-Hill and CACs of hematopoietic origin (Vasa et al., 2001; Rohde et al., 2007), ECFCs uniformly express endothelial cell surface antigens such as CD but not hematopoietic cell surface antigens such as CD45, CD14 and CD115 and display a great proliferative potential (Reinisch et al., 2009).

1.3 Cellular Imaging

While cellular behavior can easily be monitored in *in vitro* experiments, the situation *in vivo* is more complex, and is a major difficulty in regenerative medicine and cellular therapy approaches. Several key questions have to be addressed to further enhance the understanding of key mechanisms in cellular therapy.

At present it is not possible to predict the fate of transplanted cells, their distribution after injection or their engraftment level in the local environment. Despite decades of experience with hematopoietic stem cell transplantation (HSCTx) the only way to determine the efficiency of stem cell administration is still the subsequent evaluation of blood cell regeneration and chimerism by blood drawing.

Experimental stem cell therapies also lack pharmacokinetic studies as done for biologics and drugs providing information such as bioavailability and clearance from the bloodstream. This could also explain the inability to translate promising preclinical results into efficient studies. (Allan and Strunk, 2012)

Therefore it is necessary to develop appropriate noninvasive *in vivo* imaging and cell tracking tools to allow a continuous monitoring of transplanted cells. Such methods would allow the differentiation between passive stem cell trapping, active stem cell homing, engraftment and organ repopulation or regeneration. It also would elucidate the time course and the mechanisms behind those different functions. An increased knowledge of this fundamental processes could allow theimprovement of stem cell transplantation protocols regarding dose, time, conditioning and co-transplantation.

Technique	MRI	CT	PET	SPECT	Fluorescence imaging	BLI
Resolution	10-100 µm	25-50 µm	1-2 mm (dedicated small animal scanner) 5 mm (clinical system)		2-3 mm	2-3 mm
Depth	No limit	No limit	No limit	No limit	approx. 1 cm	approx. 1cm
Imaging Agent	Gd^{3+}, Mn^{2+}, Fe^{2+}, Fe^{3+}	Iodide	^{18}F, ^{11}C, ^{15}O, ^{64}Cu	^{99m}Tc, ^{111}In, ^{123}I	GFP+, NIR fluorochromes	Luciferin
Detection threshold	single cell	-	-	>10.000	single cell	approx. 1000
Current Relevance for SCI	Yes	No *	No *	Yes	Small animal models only	Small animal model only
Limitations	Long acquisition time, low specifity,	Lack of feasible cell labeling, radiation	Low spatial resolution, radiation	Low spatial Resolution	Penetration Depth	Penetration Depth

Table 1: Comparison of different imaging modalities (table modified from Kircher et al., 2011; Reinisch, 2010).

Abbreviations: MRI: Magnetic Resonance Imaging; CT: Computed Tomography; PET: Positron Emission Tomography; SPECT: Single Photon Emission Computed Tomography; BLI: Bioluminescence Imaging; SCI: Stem Cell Imaging; Gd^{3+}: Gadolinium; Mn^{2+}: Manganese; Fe^{2+}: Iron, F: Fluorine; C: Carbon; O: Oxygen; Cu: Copper; Tc: Technetium; In: Indium; I: Iodine; GFP^{+}: Green fluorescent protein and derivatives; NIR: Near infrared; * standalone device, combination with MRI or CT possible.

Possible imaging modalities can be seen in Table 1: Comparison of different imaging modalities (table modified from Kircher et al., 2011; Reinisch, 2010) and are explained in the following.

1.3.1 Optical Methods

A major drawback of imaging methods like Single Photon Emission Computed Tomography (SPECT), Positron Emission Tomography (PET), Computed Tomography (CT) or Magnetic Resonance Imaging (MRI) is the expensive equipment. Optical imaging methods require smaller devices and cheaper infrastructure but suffer from a limited tissue penetration depth due to absorption and scattering of light in the visible spectrum. Therefore the methods are only applicable in small animal imaging.

1.3.1.1 Fluorescence Imaging

In Fluorescence imaging a fluorophore is used to absorb a photon from an external light source. It enters an excited state before emitting the energy back as a photon of lower energy, which means at longer wavelength. Due to the low penetration depth of visible light photons near infrared (NIR) fluorophores are commonly used. Light within this spectral range benefits from the low absorption of hemoglobin and water between 700 and 900 nanometers wavelength and can therefore reach a penetration depth of several centimeters. Different types of fluorophores are available, such as small molecules, quantum dots or fluorescent proteins.

1.3.1.2 Bioluminescence Imaging

In contrast to fluorescence imaging, the generation of an emitted photon during bioluminescence is based on a chemical reaction of an enzyme and a substrate. No external light source is necessary. Typical systems are based on firefly luciferase and luciferin. Luciferin is a small molecule that is oxidized in the presence of the enzyme luciferase and adenosine triphosphate (ATP) to produce oxylucifern and energy in the form of a photon.

1.3.2 Computed Tomography

Computed Tomography (CT) is an important tool for medical imaging and utilizes X-rays to obtain volume density data of the investigated object with good resolution. Two major drawbacks are the lack of a feasible cell labeling method and the use of radiation. Modern application of CT makes use of the good anatomical details in combination with the high sensitivity of radionuclide based methods as explained in chapter 1.3.3.

1.3.3 Radionuclide based Methods

Although Positron emission tomography (PET) and single-photon emission computed tomography (SPECT) use γ-rays arising from radionuclide decay, they require distinct hardware and radioisotopes.

1.3.3.1 Positron emission tomography (PET)

PET systems use a positron-emitting radionuclide. As the radioisotope undergoes positive beta decay a positron is emitted. By interaction with an electron both electron and positron are annihilated and two γ-rays moving in opposite directions evolve. The PET scanner makes use of the simultaneous detection of both γ-rays to reconstruct a 3-dimensional data set. PET-systems provide a high sensitivity and possible insights into different metabolic processes depending on the chosen tracer. Due to the lack of anatomical representation it is most useful in combination with CT or MRI. Commonly used radionuclide markers (^{18}F, ^{11}C, ^{15}O and ^{64}Cu) typically show a short half-life like of 2 minutes to 12 hours.

1.3.3.2 Single-photon emission computed tomography (SPECT)

In SPECT the radionuclide itself emits γ-rays which can be detected by a gamma camera. The obtained data is then used for tomographic reconstruction. SPECT systems also provide a high sensitivity but compared to PET-scanners it is lower by two to three orders of magnitude (Rahmim and Zaidi, 2008). Radionuclides in use are ^{99m}Tc ^{111}In and ^{123}I which provide a longer half-life and are more easily obtained in contrast to PET markers.

1.4 Magnetic Resonance Imaging (MRI) Basics

Like other tomographic imaging techniques, MRI is able to produce images of internal structures of an object. However, MRI makes use of different principles of signal generation, spatial encoding and image contrast generation.

1.4.1 MRI system components

1.4.1.1 Static Magnetic Field

A supraconducting coil is used to create a static magnetic field, termed B_0. A carthesian reference coordinate system is defined in which the z-axis is aligned to B_0. The strength of this field defines the operating field strength of the MRI system and is a major determinant of the image contrast.

Local field homogeneity (shim) of all static and variable magnetic fields is an important prerequisite for accurate localization of an MR signal. Active and passive shim coils, are used to adjust the B_0 field when it is disturbed by placing an object into the MRI scanner.

1.4.1.2 Gradient and Radiofrequency (RF) Coils

Spatial localization in three directions is achieved by utilizing gradient coils. The coils lie concentric to each other and are used to create linear variations of the B_0 field. The generated magnetic gradients are very important for image formation and imaging quality. Parameters for gradient specification are the amplitude and the rise time.

Another important part of MRI is the transmission and receiving of RF energy to and from the tissue of interest. These functions are performed with coils, which are also placed concentric to each other and the gradient generating coils. There are several different types of RF coils. The type of coil mainly depends on the type of application.

1.4.1.3 Postprocessing toolchain and image reconstruction

Further steps have to be applied to the acquired set of frequency and phase data to gain an interpretable image. This includes filtering, 2- or 3-dimensional Fourier transforms to retrieve final voxel values and again different filtering steps.

1.4.2 Signal Formation

A measurable atomic nucleus has to provide a nonzero nuclear spin to achieve a magnetic moment, based on its positive charge. Hence the amount of protons and neutrons has to be unequal otherwise the spins would cancel each other. The strength of the magnetic moment depends on a physical constant called gyromagnetic ratio γ which is nucleus-dependent.

Since the nucleus of hydrogen has the simplest composition consisting of just one proton and because hydrogen is the most prominent element found in the human body, proton-based MRI is commonly used. Other candidates for MRI would be ^{13}C, ^{14}N, ^{17}O, and ^{19}F.

By putting a sample into a magnetic field, protons are aligned parallel and antiparallel to the main magnetic field B_0 with a minor excess of parallel oriented protons. The

higher the B_0-field, the higher the amount of parallel oriented protons and the resulting net magnetization of the sample will be. Therefore also the maximum signal intensity (SI) and the signal to noise ratio (SNR) of the resulting image will be increased.

To generate a signal from the sample, energy has to be delivered to the protons as a short radiofrequency (RF) pulse of particular amplitude, duration and bandwidth. The protons, aligned in the main magnetic field B_0, start to precess with a frequency ω proportional to the gyromagnetic ratio γ of the nucleus and the strength of the B_0-field. This frequency, ω, is called Larmor frequency or resonance frequency and is the characteristic frequency at which protons only absorb or radiate energy.

When the spin system is perturbed by the RF pulse, the rotating net magnetizations precess around the z, or B_0 axis. Depending on amplitude and time the net magnetization moves away from the z axis and rotate around it. The angle between the magnetization vector and the z-axis is called flip angle α. Thus the vector can be split into a longitudinal magnetization and a transverse magnetization which, as it is rotating, induces a current in the receiver coil. By turning the RF pulse off, the net magnetization vector starts to realign with the B_0-field.

Different Processes happen during re-alignment:

- First, the longitudinal magnetization recovers because the spinning nuclei release energy into the environment, which is called T1 relaxation or T1 recovery.
- Second, a process named T2-relaxation or T2 decay decreases the transverse magnetization. Spinning nuclei interact with their magnetic fields and as a result are dephased.
- A third mechanism, termed T2* relaxation or T2* decay reduces the transverse magnetization and is a consequence of magnetic field inhomogeneities.

The signal and the current, respectively, which is induced in the receiver coil, decreases as the spins dephase and is called free induction decay (FID). In general, the acquired signal is called echo.

1.4.3 Signal localizing and encoding

To encode the signal spatially, gradients are applied, which vary linear over the required field of view (FOV) and perform three functions depending on their spatial orientation.

The gradient along the z-axis (same direction as the static B_0 field) allows a slice selection whereas the gradients along the x- and y- axis are used to further resolve localization information out of the selected slice. The gradient in x-direction is used to imprint a linear variation of the protons resonance frequency within a slice, whereas the gradient along the y-axis induces a linear phase shift of the magnetization across the selected slice during the readout of the signal.

By combining these three different gradients in a pulse sequence a specific frequency and phase is imprinted on every single spin in the targeted tissue and permits a spatial correlation. Each sequence pass echo returns information about on line within a selected slice, whereas the thickness of the slice and the dimension of the line, respectively the voxel dimension is determined by the RF pulse bandwidth and the gradient steepness.

The obtained data are stored as complex numbers within a matrix, a representation called the k-space. This representation depends on the sequence used for image acquisition and holds the raw frequency and phase data. To generate an anatomical image these data has to be further processed to generate an appropriate image and can be further modified by application of different mathematical operations for further contrast enhancement or volume rendering.

1.4.4 Image Contrast and Pulse Sequences

MRI contrast is mainly dependent on the difference in signal intensity among adjacent tissues. Signal intensity itself further depends on multiple parameters including spin or proton density, innate tissue T1 and T2 relaxation times, the presence of natural or artificially applied paramagnetic ions, and diffusion or perfusion of imaged water molecules in and out of voxels during scan time. Above all, T1, T2 and proton density are mainly used to generate imaging contrast. These factors are controlled by two key parameters, time of echo (TE) and repetition time (TR). By adjusting them properly it

is possible to emphasize either T1, T2 or proton density properties of the targeted tissue.

A large number of sequences has been developed to emphasize diffusion or perfusion processes, but many of them are derived from gradient recalled echo sequences and spin echo sequences. The third sequence introduced here gives an insight to the sequence used for the MRI-experiments in this thesis.

1.4.4.1 Spin echo (SPE) sequences

This sequence generates spin echoes by the application of a 180° refocusing RF pulse after the 90° excitation pulse. After application of a 90° RF pulse the spins are tipped into the transverse plain and start dephasing due to T2 and T2* processes (Figure 2, A). While dephasing evoked by T2 relaxation is an irreversible and random process, T2*-caused relaxation by the presence of static magnetic field inhomogeneities is reversible. Thus the application of a 180° refocusing pulse at the time point TE/2 rotates the spins, effectively turns the direction of dephasing (Figure 2, B). Hence the spins come back in phase to reach a maximum signal at the time point TE (Figure 2, C). (Ridgway, 2010)

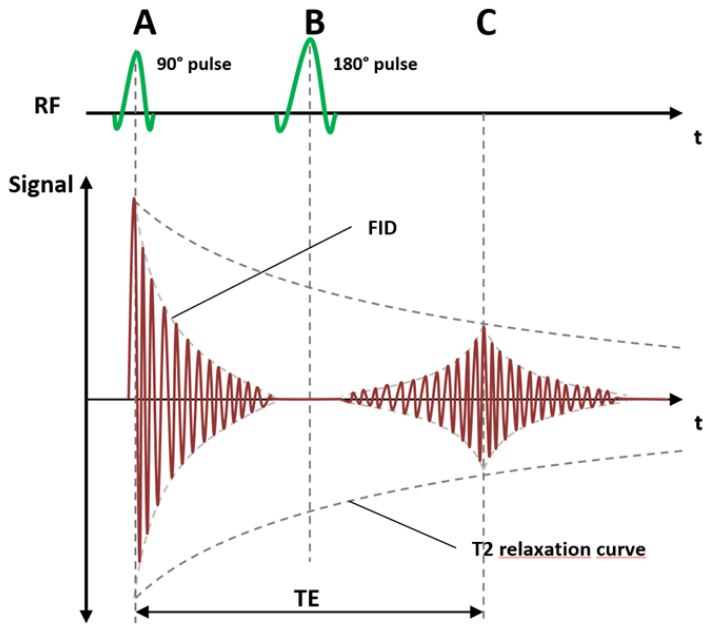

Figure 2: Sequence diagram. Generation of a spin echo. **A:** A 90 degree (90°) excitation pulse creates a free induction decay signal (FID). **B:** At the half time of echo (TE), a 180 degree (180°) excitation pulse is used to invert dephased spins. **C:** The spins realign after full TE with a maximum amplitude based on T2 relaxation.

1.4.4.2 Gradient recalled echo (GRE) sequences

As the name implies, GRE based sequences use a gradient to rapidly dephase spins along the gradients direction to destroy the FID signal. Starting with the RF excitation pulse a gradient is turned on and the spins loose coherence (Figure 3, A). This causes the amplitude of the FID signal to rapidly decrease to zero (Figure 3, B). By applying a second gradient for the same amount of time and with the same amplitude in opposite direction, the phases of the spins regain coherence and start to rebuild the FID signal (Figure 3, C). After the double amount of time the signal is destroyed again (Figure 3, D). (Markl and Leupold, 2012; Ridgway, 2010)

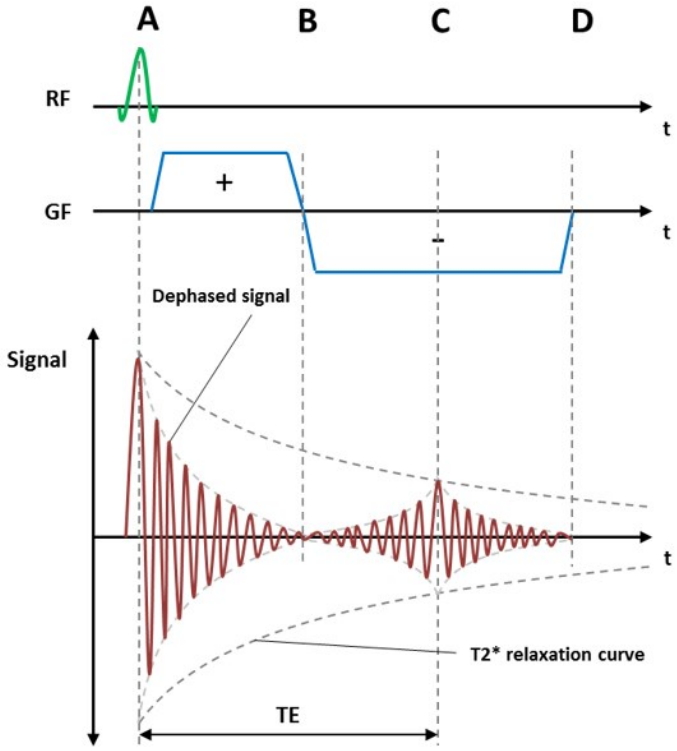

Figure 3: Sequence diagram. Generation of a gradient recalled echo. A: An excitation pulse deflects the spins. At the same time a gradient field is turned on to rapidly dephase the spins thus destroying the signal. **B:** The gradient direction is inverted after half time of echo (TE). **C:** At TE the spins rephase and reach a signal maximum depending on T2* relaxation. **D:** The inverted gradient remains to destroy the signal again. A new sequence repetition can be started.

1.4.4.3 Ultra-short time of echo (UTE) sequences

UTE imaging is currently investigated in a clinical setting for tissues containing a majority of short T2 components like cortical bone, tendons, ligaments and menisci since conventional clinical pulse sequences are not able to gain appropriate signals

from these tissues due to high echo times. Such sequences have generally not been available in the past due to high scanner requirements but are entering clinical imaging as suitable scanners are spreading and experience and studies are increasing (Bydder, 2011). While standard T1 contrast agents usually provide relaxivity of approximately 5 $mM^{-1}s^{-1}$ for both r1 and r2, sensitivity can be increased with superparamagnetic iron oxide (SPIO) or ultrasmall superparamagnetic iron oxide (USPIO) contrast agents which provide greater r1 and r2 relaxivity. As a consequence of a high r2 value the relaxation time T2 is short, thus the MR signal is destroyed faster. Therefore shorter echo times are required to make use of it. Another consequence of ultra-short echo times is the reduced influence of normal tissue on contrast. This can be further used to highlight the impact of the contrast agent.

A GRE-based, fast low angle shot (FLASH) sequence, was used as base for the UTE imaging. SPE and GRE sequences turn the net magnetization vector (NM) by 90 degrees into the transverse plane. The excitation RF pulse of the UTE-sequence deflects the NM by the flip angle α away from the longitudinal axis. This results in a shorter time for the recovery of the NM thus reducing TR. As a consequence of the trigonometric dependency, a high transverse component of NM, can still be achieved.

The signal acquisition happens directly after the RF pulse. Concurrently a readout gradient in all three directions is applied to imprint spatial information (Figure 4, A). Repetition time is further decreased by adding a spoiling gradient after the acquisition to dephase the remaining transverse component (Figure 4, B).

A balanced steady-state free precession (bSSFP) sequence, termed balanced UTE (bUTE) was also used for imaging. The flip angle α is applied positive and negative in an alternating manner making a spoiling gradient unnecessary. (Figure 4, C and E). During acquisition two readout gradients are applied for spatial encoding and the generation of two echos (Figure 4, D). Both echos can be used for image generation thus doubling the acquired image data per sequence pass. This results in an increased contrast to noise ratio (CNR).

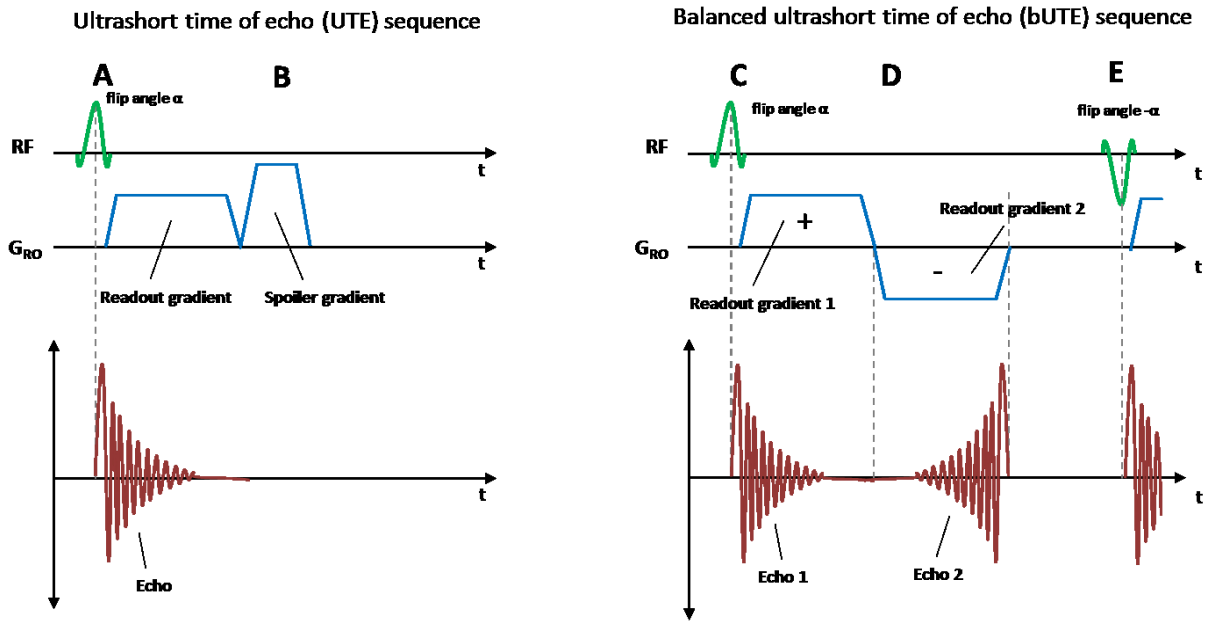

Figure 4: Diagrams of two different ultrashort time of echo sequences. Both sequences are based on a gradient recalled echo sequence **UTE sequence: A:** An excitation pulse of flip angle α is turned on. The signal is acquired directly using the readout gradient. **B:** A spoiler gradient is used to destroy the transversal signal. **bUTE sequence**: **C:** An excitation pulse of flip angle α is used for spin rotation. A concurrent positive readout gradient is used to acquire a first echo (Echo 1). **D:** The gradient is inverted to generate a second echo (Echo 2). This doubles the information retrieved within on sequence pass. **E:** Instead of a spoiling gradient, the next pass uses an inverted pulse (flip angle -α) thus switching the net magnetization into the opposite direction and preventing an accumulation of remaining longitudinal magnetization.

During the work on this thesis, the UTE sequences were optimized to emphasize the possibilities of SPIO and USPIO MR contrast agents. A 3D radial imaging approach was used to gain a small voxel volume. This increases the relative contribution of a contrast agent to the total signal acquired from each voxel. Another benefit of the approach is the insensitivity to motion artifacts.

A comparison of the described sequences can be seen in Figure 5. TSE and GRE are both 2D sequences. While TSE is insensitive to motion, GRE shows noticeable artifacts. Although both sequences provide a good two-dimensional resolution and a shorter imaging time, the voxel volume is increased. UTE and bUTE were acquired using a 3D radial imaging approach with a voxel size of 160^3 µm. Two slices were combined to gain an increased CNR resulting in a voxel size of 160 x 160 x 320 µm. The reduced TR of UTE and bUTE is used to acquire more volume data compared to SPE and GRE to gain a higher CNR.

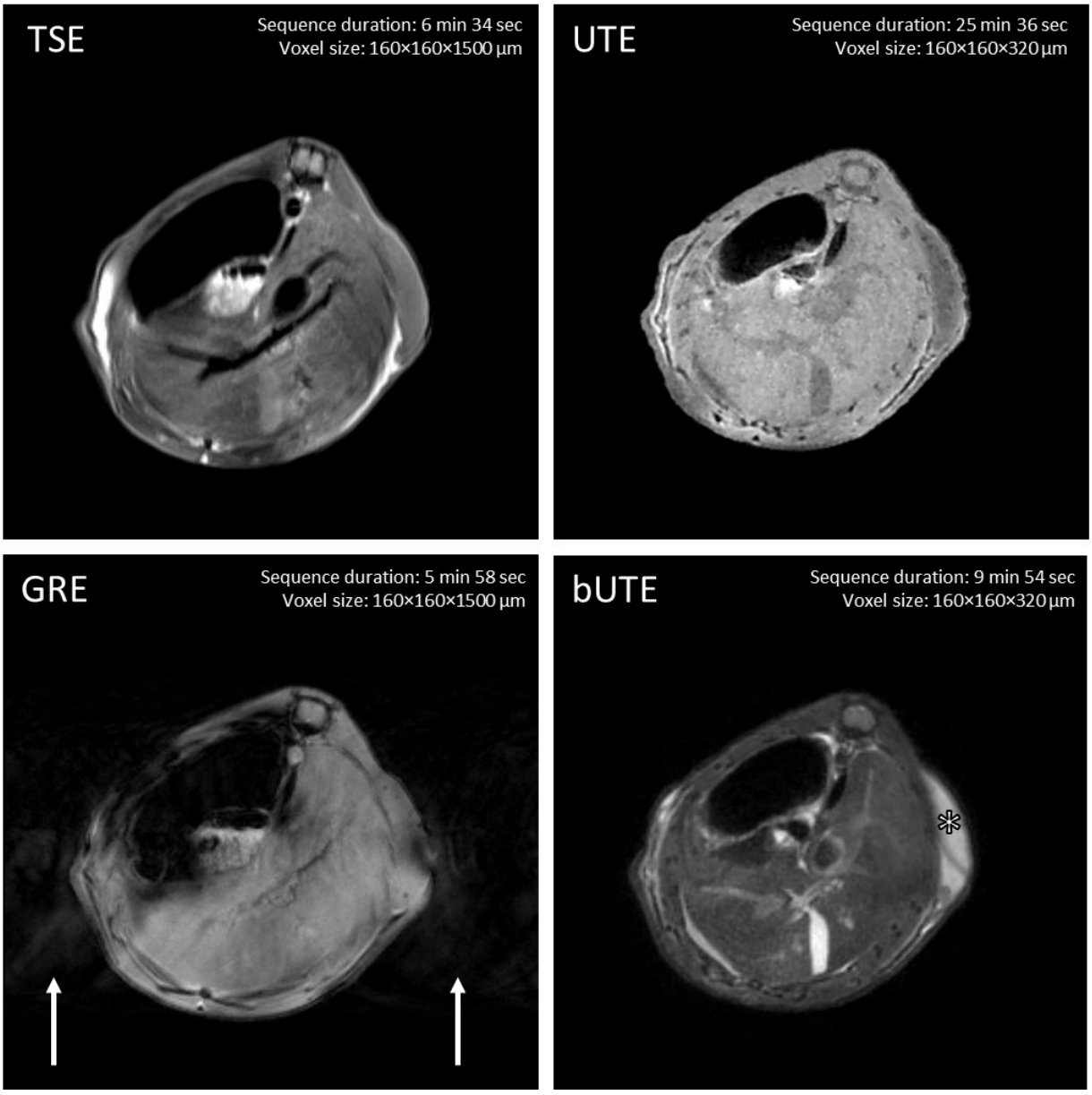

Figure 5: Comparison of different MRI sequences. TSE and GRE sequence were acquired slice by slice in two dimensions (2D) while UTE and bUTE utilized a three dimensional approach enabling higher resolution in all spatial directions. Total sequence duration and voxel size are given for each sequence. **TSE**: turbo spin echo sequence. TSE sequences provide excellent T1 contrast and are relatively insensitive to motion artifacts **GRE**: gradient recalled echo sequence. GRE sequences are sensitive to motion (arrows) but provide a broad spectrum of possible contrast. **UTE**: ultrashort time of echo sequence. UTE sequences are very insensitive to motion artifacts and provide high resolution. **bUTE**: balanced UTE sequence. Another UTE-sequence which was further optimized to provide homogenous tissue contrast to focus especially on cell tracking within the implanted plug (star).

1.4.5 Contrast Agents for Magnetic Resonance Imaging

MRI contrast agents must have the ability to efficiently lower the T1 and/or T2 in tissues at low concentrations. This fundamental ability is referred to as the contrast agents relaxivity r1 and r2. An agent with a higher relaxivity will lower T1 and/or T2 more at equal concentrations than an agent with a lower relaxivity. Therefore contrast agents with high relaxivity can permit the generation of an increased signal at the same field strength, the usage of lower dose resulting in a reduced toxicity and an improvement in detection of lesions or, as in this case, targeted cells. (Hao et al., 2012)

1.4.5.1 T1 Contrast Agents

The most prominent and most frequently used clinical MRI contrast agent is based on Gadolinium. Gadolinium and also Manganese based contrast agents alter primarily the longitudinal (T1) relaxation rate. Their unpaired electrons provide a magnetic moment, which increases the relaxivity. This shortens the T1 relaxation and therefore increases the signal on T1-weighted MRI sequences, resulting in a “positive”, hyperintense contrast.

The MRI signal change caused by these agents is usually not large enough to visualize a small number of cells because of the low relaxivity ranging from 3 to 8 $mM^{-1}s^{-1}$ for both r1 and r2 (Hao et al., 2012). This parameters can further be increased by optimization of the contrast agents vicinity through alteration of binding groups (Jacques et al., 2010). Another possible drawback of Gadolinium based agents is the strong inverse field dependent relaxivity. This results in a decreased influence of the contrast agent on image contrast when used with upcoming preclinical 7 to 9.4 T MRI scanners compared to common 3 T devices.

1.4.5.2 T2 Contrast Agents

The principal effect of T2 contrast agents is the tissue signal loss, due to the susceptibility effects of the particles’ iron oxide core. This reduces the signal intensity of labeled cells or tissue and darkens the image. Therefore SPIO particles are also classified as negative contrast agents. Due to the property of superparamagnetism the iron oxides agents are referred to as superparamagnetic iron oxide (SPIO) (Kraitchman and Caravan, 2009). Iron oxide contrast agents provide an inherently larger effect on

MRI relaxivity and thus are predominantly used in current MRI based cell tracking approaches. The relaxivity can be further increased by altering the particle surface. By covering an iron oxide particle with thiolated polyacrylic acid it was possible to at least double the relaxivity values of Resovist® (Vetter et al., 2011).

The particles are grouped based on their size into superparamagnetic iron oxide (SPIO, 50 - 100 nm) and ultrasmall superparamagnetic iron oxide (USPIO, 10 - 50 nm).

Trade name	**Hydrodynamic diameter (nm)**	**Core**	**Shell/Coating**	**Relaxivity ($mM^{-1}s^{-1}$)**	
				R1	R2
Resovist® (Ferucarbotran)	~ 62	Fe_3O_4/Fe_2O_3	Carboxydextran	19,4	185,8
Molday Ion™	~ 30	Fe_3O_4	Hydroxyl	36,4*	70,6*
Molday Ion™ (-)	~ 30	Fe_3O_4	Hydroxyl	n/a*	n/a*
Molday Ion™ CT	~ 35	Fe_3O_4	Carboxyl	n/a*	n/a*

Table 2: Properties of used iron oxide particles

* Relaxation values as published (Ernest, 2011). No specification could be found for Molday Ion™ (-) and Molday Ion™ CT but they are considered to be in the range of 30 - 40 $mM^{-1}s^{-1}$ for R1 and between 60 and 75 $mM^{-1}s^{-1}$ for R2 (values are an estimation based on other Molday Ion™ Products)

Currently used iron oxide contrast agents exhibit superparamagnetic properties. Superparamagnetic iron oxide nanoparticles provide a high magnetic susceptibility because single crystals can be formed at the nanometer size scale consisting of just one magnetic domain. In contrast, large magnetic nanoparticles typically consist of multiple magnetic domains that are not well aligned. Thus the domains interfere with each other, even within a superimposed magnetic field. Despite their large magnetic susceptibility, superparamagnetic iron-oxide particles do not exhibit a magnetic remanence in absence of a magnetic field due to Brownian fluctuations that are strong

enough to randomly orient the single magnetic moments so that the bulk solution has no net magnetization.(Gossuin et al., 2009).

In opposite to T1 contrast agents iron oxide probes shorten T2 regardless of the cellular location or the amount water in close proximity (Bulte and Kraitchman, 2004).

The internalization of SPIO and USPIO is based on receptor mediated endocytosis and metabolization takes place via the lysosomal pathway. The biodegradable composition of particles permits an integration of iron into the somatic iron pool.

1.4.5.2.1 Ferucarbotran (Resovist®)

This SPIO was commercially (Bayer Schering Pharma, Berlin, Germany) available until 2009 and was FDA-approved for liver tumor imaging. The Resovist core is made from magnetit (Fe_3O_4) and maghemite (Fe_2O_3) microparticles. A carboxydextran coating ensures aqueous solubility of the particles and prevents aggregation (Reimer and Balzer, 2003)

1.4.5.2.2 Molday Ion™ Family

Molday Ion product family (BioPhysics Assay Laboratory, Inc., Worcester, Massachusetts) comprises several different USPIO contrast agents mainly developed for cardiovascular and vascular research. The core is based on magnetit (Fe_3O_4) nanoparticle. More detailed information about the composition and the coating of the particle could not be found. All currently available properties can be found in Table 2. The rationale for the utilization of Molday Ion™ products was the supposed greater contrast enhancement in comparison with the SPIO Resovist when used together with UTE imaging sequences. (Ernest, 2011)

1.4.6 Labeling techniques

1.4.6.1 Indirect labeling

Indirect labeling methods make use of a reporter gene that is introduced into a cell and translated into enzymes, receptors or fluorescent or bioluminescent proteins.

These enzymes and receptors can then be used to enrich an unspecific, systemically applied label or specifically bind a conjugated contrast agent to the target cell.

Ideally, if the expression of the introduced reporter gene is stable, the labeled cell can be observed over the entire lifetime. As the reporter gene is usually also handed over to its progeny cells, it is possible to image expanding cell populations over time.

Nevertheless it is possible to have negative effects on cell labeling like gene silencing owing to DNA methylation or histone modification which affects transcription and suppress the reporter signal (Bengtsson et al., 2011; Velde et al., 2013).

The indirect labeling of cells requires genetic modifications of the cellular genome. A strict evaluation of modified cells is necessary to ensure an unchanged cellular phenotyp and function. Due to the sound proliferation and differentiation potential of stem/progenitor cells this safety concerns have to be covered in future studies. This is crucial especially when modified cells are designed for human application to avoid unwanted tumorigenesis as reported (Mukherjee and Thrasher, 2013)

1.4.6.2 Direct labeling

Whereas indirect labeling involves greater effort, a direct attempt to label cells can be carried out fairly simple. A cell population is labeled by *in vitro* incubation with a suitable MRI contrast agent. The cells can then be used for *in vivo* application or further testing *in vitro*.

Several disadvantages occur when using a direct labeling method. It is possible to impair the cellular function, phenotype or differentiation capacity (Farrell et al., 2008; Yang et al., 2010; Cromer Berman et al., 2013). Another drawback is the dilution of the label during symmetric or asymmetric cell division. The cell label can even get lost and taken up by phagocytic cells which greatly reduces specificity (Gonzalez-Lara et al., 2010; Lassailly et al., 2010; Mani et al., 2008). Despite this drawbacks, direct labeling of MSC has been reported as efficient strategy for cellular tracking without influence on cellular function, phenotype or differentiation. (Arbab et al., 2005; Gerlinde Schmidtke-Schrezenmeier et al., 2011; Janic et al., 2009)

1.4.6.2.1 Transfection agents

To optimize direct uptake of cellular labels, transfection agents are commonly used. These are positively charged molecules like Superfect, Dioleoyloxy-trimethylammonium-propane (DOTAP), Lipofectamin, poly-L-lysine (PLL) or protamine-sulfate (PS). A higher concentration of these transfection agents is toxic and

only protamine-sulfate is clinically approved as antidote against heparin overdosage. (Arbab et al., 2004)

The transfection agents and contrast agents assemble via electrostatic interactions. Every combination of (U)SPIO and agent has to be titrated and optimized carefully. Lower concentrations may yield to insufficient uptake of particles whereas higher concentrations may result in precipitation of complexes or may be toxic to the cells (Arbab et al., 2004).

For this thesis protamine-sulfate and poly-L-lysine were used but the main focus was on protamine-sulfate due to its FDA approval.

1.4.6.3 Liposome based labeling

Currently, Liposomes of different composition are investigated as drug delivery agents. They are currently also observed in detail as delivery agent for contrast agents.

MRI contrast enhancement with SPIO contrast agents depends on the size and the concentration of SPIO particles within a certain space. Micrometer-sized Liposomes allow high concentrations of SPIO particle within a cell with minimum cytotoxicity which has been the rationale for the examination of Liposomes as contrast agents for single cell imaging of fish embryos (Toyota et al., 2012).

Liposomes have already been analyzed as transfection agent for SPIO labeling of pancreatic islet cells without affecting the function or viability of the cells (Jiao et al., 2008). They have also been tested as *in vitro* and *in vivo* tumor-targeting imaging probe for human cancer cells (Yang et al., 2008).

The Liposomes used for this thesis were developed at the Institute of Biophysics and Nanosystems Research, Austria Academy of Sciences by Daniela Frascione. The magnetic liposomes (ML) consist of a Palmitoyl-Oleyl-Glycero-Phosphocholine (POPC) surface and encapsulate Molday Ion™ USPIOs. The POPC-vesicles were analyzed with respect to their chemical, physical and imaging characteristics (Prassl et al., 2012).

2 Materials and Methods

2.1 Ethics statement

Prior approval was obtained for all human cell and tissue sample collection from the Institutional Review Board of the Medical University of Graz (protocols 19-252 ex 07/08, 18-243 ex 06/07 21-060 ex 09/10). Umbilical cord and umbilical cord blood samples were collected after informed consent of the mother after full-term pregnancies in accordance with the Declaration of Helsinki. All Animal experiments were authorized by the Animal Care and Use Committee at the Veterinary University of Vienna on behalf of the Austrian Ministry of Science and Research.

Blood samples were obtained after written informed consent in accordance with the declaration of Helsinki. The study protocols were approved by the institutional review board of the Medical University of Graz (protocol numbers 19-252 ex 07/08 and 18-243 ex 06/07)

2.2 Preparation of cell culture medium

2.2.1 MSPC-Medium

Medium was prepared as described (Schallmoser et al., 2007). Briefly, 500 mL of α-modified minimum essential medium (Sigma-Aldrich) was supplemented with 2 IU/mL of preservative-free Heparin to avoid clumping of the fibrinogen in the plasma and admixed with 56 mL of pooled human platelet lysate (pHPL). Additionally a Penicillin (100 IU/mL)/Streptomycin (100 µg/mL) solution and 2 mM of L-glutamine (both Sigma) were added. Finally the medium was filtered through a 0.22 µm-pore size vacuum filter (Millipore). The supplemented medium is referred to as α-MEM.

2.2.2 ECFC-Medium

The endothelial growth medium was prepared as described (Reinisch et al., 2009). Before supplementing with 56 mL of pHPL, 10 IU/mL of preservative-free heparin was added to avoid clumping of the fibrinogen in the plasma. Cytokine-aliquots (human vascular endothelial growth factor [hVEGF], human basic fibroblast growth factor

[hbFGF], human epidermal growth factor [hEGF], insulin-like growth factor-1 [IGF-1], hydrocortisone, acrobic acid), Penicillin (100 IU/mL)/Streptomycin (100 µg/mL) solution and 2 mM of L-glutamine were supplemented and the medium was then filtered through a 0.22 µm-pore size vacuum filter.

2.3 Cell Isolation and propagation

2.3.1 ECFC

The umbilical cord was washed twice with pre-warmed PBS and rinsed to get rid of contaminating blood cells. The cord was then transferred in a new culture plate and cut into pieces of 5 cm length. The umbilical vein was then cut longitudinally and transferred in another culture plate. After that, a cell scraper was used to scrape the endothelial surface of the vein at least ten times. The tip of the scraper was cleaned each time in a prepared pHPL-supplemented EGM-2-filled 75mm2 flask to transfer cells. The flask was then closed and put into an incubator at 37°C with 5% CO_2 and 95% Humidity. The supplemented EGM-2 medium was replaced on the next day to get rid of non-attached cells. The cells were expanded until reaching confluence and were detached using 0.25% trypsin/1 mM ethylenediaminetetraacetic acid (EDTA). Further expansion of the cells was performed using a low seeding density. One third of the medium was exchanged twice a week until reaching confluence. Cells where harvested by trypsinisation and 1 x 10^6 Cells per vial were resuspended in pHPL-supplemented EGM-2 with 10% v/v dimethyl sulfoxide (DMSO) and cryopreserved in liquid nitrogen using for further use. (Reinisch and Strunk, 2009)

2.3.2 MSPC

MSPC were isolated from both umbilical cord (UC) and bone marrow (BM) and are herein termed UC-MSC and BM-MSC. UC-MSC isolation was subsequently performed after the ECFC-isolation. After scraping off the endothelial layer the whole piece of umbilical cord was cut into 1-2 mm parts using a sterile scissor and scalpel. The cord pieces were then transferred into culture plates. To enhance the attachment of the pieces the plate was left open for 5 minutes before 30 mL of pre-warmed α-MEM were gently added. The plate was then closed and put into an incubator at 37°C with 5%

CO_2 and 95% humidity. Cells were harvested when reaching confluence greater 80-90% by trypsinisation (Reinisch et al., 2007).

BM collection was performed after written informed consent according to protocols approved by an institutional review board. Both compartments of the bone marrow aspirate concentration (BMAC) container were 'washed out' by rinsing with a total volume of 50 mL pHPL-supplemented α-MEM. 5 mL of each compartment were seeded into a 6-well plate in different concentrations for visualization of colony forming units of fibroblasts (CFU-F) indicating mesenchymal stem and progenitor cell (MSPC) frequency. The remaining 45 mL from the BM concentrate part of the container were seeded into a T225 flask. The other 45 mL from the top part of the BMAC container were diluted with 355 mL pHPL-supplemented α-MEM and seeded into one four-layered cell factory (CF-4; Thermo Fisher). Expansion was done as described. In brief, cell culture medium was displaced, the cells were washed with 37°C prewarmed PBS two times before adding new pHPL-supplemented α-MEM. Cultures were fed twice a week by replacing one third of the old medium with new MSPC-Medium. Cells were harvested when reaching confluence greater 80-90% by trypsinisation (Bartmann et al., 2007).

MSPC from both sources were resuspended in pHPL-supplemented α-MEM with 10% v/v dimethyl sulfoxide (DMSO) and cryopreserved in liquid nitrogen for further experimental use.

2.4 Cell labeling

Resovist®, different Molday Ion™ species and iron-containing liposomes were used for progenitor cell labeling.

Labeling procedure with Resovist® was performed as described (Arbab, 2004, Janic et al., 2009). Minor modifications were performed to further enhance the uptake of Resovist®. In brief, Resovist® and PS were added to serum-free RPMI-1640 medium to avoid complex formation between SPIO/PS and serum proteins (Reinisch, 2010). After 20 minutes of incubation at 37°C an equal amount of cellular culture medium was added to achieve a final concentration of 10 to 200 µg iron/mL and 3 µg/mL of protamine sulfate, respectively. The fresh SPIO-containing medium then replaced the old culture medium and the cells were incubated for 24 hours.

Molday Ion™ labeling was performed with different USPIO surface modifications as described by the manufacturer (BioPAL, 2013). In brief, different concentrations of PLL were mixed with Molday Ion® and distilled water to reach a concentration of 100 µg iron/mL and incubated for one hour. Cells were labeled by using equal volumes of prepared labeling solution and standard culture medium overnight.

To further evaluate optimum labeling conditions, different concentrations for both the USPIOs and the transfection agents were tested. The USPIO and either PLL or PS were added to serum-free RPMI-1640 medium. The labeling reagent was then incubated for one hour at 37°C and mixed with an equal amount of cell culture medium afterwards to reach a final labeling concentrations between 10 and 1000 µg iron/mL and 5 and 500 µg/mL of PS or PLL respectively. The prepared labeling reagent was then used to replace the old culture medium and the cells were incubated for 24 hours.

Another approach of labeling was to utilize palmitoyl-oleoyl-phosphatidylcholine (POPC) liposomes as delivery system for both SPIO and USPIO particles (Prassl et al., 2012). (Liposomes were kindly provided by Daniela Frascione, Institute of Biophysics and Nanosystems Research, Austrian Academy of Sciences, Graz.)

Fluorescein isothiocyanate (FITC) and ATTO 655 (ATTO-TEC GmbH, Germany; www.atto-tec.com) were tested as fluorophores for liposome visualization. Both fluorophore-conjugated liposome species were further tested with and without polyethylene glycol (PEG) modified surface.

The different empty, SPIO or USPIO containing liposome species were first tested and added at concentrations of 100, 500 and 1000 µg POPC/mL to prewarmed standard culture medium. Cells grown to 90% confluence were then incubated overnight. For liposomal visualization by fluorescence microscopy cells were cultured in 2 chamber slides.

Following incubation with labeling solution, the cells were either fixated for imaging purposes or were washed three times with prewarmed PBS and harvested using 0.25% trypsin/1 mM EDTA. Viable cell number was evaluated using a hemocytometer as the mean of two measurements together with Trypan Blue exclusion of non-viable cells.

2.5 Detection of particle uptake

2.5.1 Visualization of iron uptake

The uptake of iron was visualized using Prussian Blue Staining. For this purpose cells were cultured in chamber slides and labeled as described (Reinisch, 2010). The cells were fixed with 4% formaldehyde for 20 minutes. The staining solution was prepared using equal volumes of 4% Potassium-Ferro-Cyanide and 1% hydrochloric acid and the cells were incubated for 10 minutes. Cell nuclei were stained with 0.1% nuclear fast red aluminium sulfate solution. Slides were then covered with appropriate mounting medium and glass.

2.5.2 Visualization of liposome uptake

Cells were either labeled with FITC and ATTO 655 conjugated liposomes, with PEG-ylated und unmodified surface, empty or filled with SPIO and USPIO. After the labeling step cells were fixed with 4% formaldehyde for 20 minutes. FITC conjugated liposomes were further labeled with CellMask™ Deep Red plasma membrane stain (Invitrogen) according to the manufacturer's instruction. A diamidino-phenylindole (DAPI) containing mounting media (Vectashield Mounting Medium, Vector Labs), was used for visualization of cellular nuclei prior coverage by a covering glass. Pictures were made on an Olympus BX51 inverted microscope with a Color View III camera and further processed using Analysis B Software (Olympus).

2.5.3 Photometric quantification of intracellular iron concentration

To measure cellular iron content in a magnetic resonance independent manner a spectrometric method was used (Rad et al., 2007). Cells were labeled with 3.3, 10, 30, 90, 270 µg iron/mL as described above and washed with PBS thoroughly. The preparation steps were performed in triplicates. Following harvesting, 3 x 10^5 cells of each labeling concentration were put in tubes and centrifuged at 735 x g for 5 minutes. The supernatant was discarded and the remaining pellet was dried in the open tube at 110°C overnight. The pellet was then resuspended extensively with 5M hydrochloric acid and was left at 60°C for 4 hours within the now opened tube to allow a dissolving of iron. For absorbance measuring 100 µL of each sample were transferred to a 96-

well plate. A standard calibration line was prepared containing from zero to 16 µg iron/mL and absorbance for was measured at 351 nm as described in the protocol. Iron concentration of the solution was determined by normalizing with the previously prepared calibration line. The iron concentration was then divided by the number of cells to obtain the iron concentration per cell.

2.6 Cell function

2.6.1 MSPC Differentiation

Cells were precultured into 225 cm^2 flasks with supplemented α-MEM at a density of 1000 to 10000 cells/cm^2 at 37°C, 5% CO_2, and 95% humidity until they reached 90% confluence. For adipogenic and osteogenic differentiation assays cells were cultured in 6-well plates and in a 24-well plate with insert for chondrogenic differentiation, respectively. Cell Differentiation was induced by medium replacement with differentiation medium. Medium was then changed twice a week

To induce adipogenic differentiation cells were incubated in a medium prepared as follows: 45mL of Mesencult™ MSC Basal Medium was supplemented with 5 mL of MesenCult™ Adipogenic Stimulatory Supplement, 1 mL Penicillin (100 IU/mL)/Streptomycin (100 µg/mL) solution, 1 µM Dexamethason, 100 µM Indomethacin, 10 µg/mL Insulin and 0.5 mM 3-isobutyl-1-methylxanthine (IBMX). Cells were kept in culture for 3 weeks. Cells were then washed with PBS and fixed with 4% formaldehyde. Staining of intracellular lipid accumulation was performed with Oil Red O (0.5% stock solution in 2-propanol, 3:2 solution in distilled water) for 25 minutes (Reinisch, 2010).

To induce osteogenic differentiation 42.5 mL of Mesencult™ MSC Basal Medium was supplemented with 7.5 mL of MesenCult™ Osteogenic Stimulatory Supplement, 5 µL of 10^{-4} M stock solution of dexamethason, 250 µL of 10 mg/mL ascorbic acid solution and 175 µL glycerol-2-phosphate. After 10 days in culture, alkaline phosphatase activity was assayed by histochemical staining (alkaline phosphatase kit No.85, Sigma) following the manufacturer's protocol (Reinisch, 2010).

For chondrogenic differentiation cells were grown in MesenCult™ MSC Basal Medium supplements with 100 µM dexamethason, 40 µg/mL prolin, 25 µg/mL ascorbic-2-phosphate, 100 µg/mL sodium-pyruvate, 10 mg/mL transforming growth factor-β3

(TGF-β3) and ITS+1 (Insulin-transferrin-selenium, linoleic acid). Cells were cultured in a 24-well plate in the upper compartment of a Transwell insert. Chondrogenic differentiation was visualized by staining of mucopolysaccharides and glycosaminoglycans with Alcian Blue. Cell pellets were cut out of the insert, fixed with 4% formaldehyde for 48 hours embedded in paraffin. Sections were de-paraffinized by a descending alcohol series (2x xylol, 10 min; 1x ethanol 100%, 5 min; 1x ethanol 90%, 5 min; 1x ethanol 70%, 5 min; 1x ethanol 50%, 5 min; 1x PBS, 5 min) and stained with Alcian Blue (1% Alcian Blue in 3% acetic acid solution, pH 2.5) for 30 minutes (Reinisch, 2010).

2.6.2 ECFC network formation

In vitro vascular network formation was tested as previously described (Rohde et al., 2007). Briefly, cells were transferred into 16-well chamber slides (Lab-Tek®, Nunc) pre-filled with 50 µl Matrigel® (Chemicon) and cultured for 12-24 hours. In the case of vascular network preparation, 75,000-100,000 SPIO-labeled ECFCs were cultured in two-well chamber slides (Lab-Tek®, Nunc). The vascular network branches were photographically documented with a Zeiss microscope equipped with a motorized table to be capable of multi picture acquisition with subsequent aligning (Rohde et al., 2006).

2.7 Animal Experiments

(Mouse experiments were performed together with Dr. Andreas Reinisch, MD/PhD)

The Animal experiment was approved by the Animal Care and Use Committee at the Veterinary University of Vienna on behalf of the Austrian Ministry of Science and Research (Bundesministerium for Wissenschaft und Forschung, BMWF) according to the criteria published in the Guide for the Care and Use of Laboratory Animals by the National Institutes of Health (NIH publication 86-23, revised 1985). A 24 week old highly immune-compromised mouse (NOG mouse [NOD-SCID, IL2-receptor γ-chain$^{-/-}$], NOD.Cg-Prkdc^{scid}Il2rg^{tm1Wjl}/SzJ, The Jackson Laboratory, Main, USA; www.jax.org) was used as recipient to prevent immune-mediated cell rejection. The mouse was kept under specific pathogen free (SPF) conditions.

MSPCs and ECFCs were combined at a ratio of 80:20 with a total count of 2x10^6 cells and admixed with either 10 000, 2000, 400 or none Resovist® labeled ECFCs to assess the *in vivo* cell tracking sensitivity and imaging performance provided by the UTE MRI sequence.

On day 0, cells were resuspended in Matrigel® (Chemicon) and put on ice until implantation. The implantations were performed at day 0 under anesthesia of the mouse according to the approval for animal handling (BMWF:-66.010/0082-II/10b/2009). Plugs were generated by injection of 300 µL Matrigel containing 2x10^6 cells subcutaneously into the flank next to fore- and hind limb on both sides as can be seen in Figure 6.

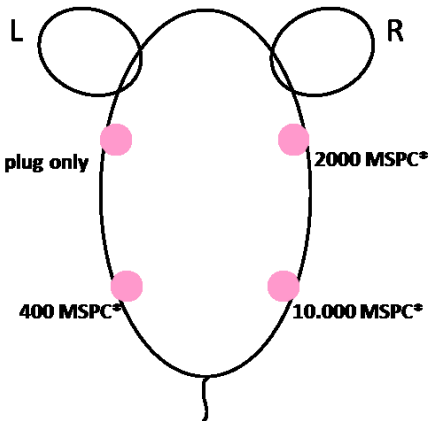

Figure 6: Position of labeled cell plugs injected at day 0.

MR imaging was performed at day -1, 0, 7, 14 and 21 under anesthesia. The mouse was euthanized at day 21. The 4 plugs were excised and immediately fixed in 4% formaldehyde.

2.8 MRI sequences and measurements

(Sequence implementation and MRI operation was performed by Clemens Diwoky, Institute of Medical Engineering, Technical University of Graz.)

For evaluation of optimal labeling and determination of detection limits with MRI, a phantom featured with properties that provide optimal human tissue comparable magnetic properties was used. Briefly, 50 mL polycarbonate tubes filled with 1% low melting point (LMP) agarose gel (Invitrogen) and 0.15 mM Gadolinium chelated with diethylene triamine pentaacetic acid (DTPA) and 0.05 mM Resovist were admixed to reach appropriate T1 and T2 values of 1074/66 ms.

Cavities for cell placement were made by placing 5 mm NMR tubes into the hardening agarose to leave space for cell placement. Equal amounts of cell suspension and 2% LMP agarose were resuspended to reach the final cell concentration in 1% LMP agarose. After gel solidification and tube removal, cell suspensions were transferred into the cavities.

The MR sequence was implemented on a 3T Tim TRIO clinical MR scanner (Siemens, Erlangen) at the Medical University of Graz. A volume coil with an inner diameter of 3.5 cm was used for all experiments. The single-cell phantom was scanned with the scan parameters TR = 7.5 ms, flip angle α = 29°, FID = 0.1 ms, LE = 7.3 ms at a matrix size of 256^3 resulting in an acquisition time of 8 min 15 s for each whole volume scan. *In vivo* images were acquired at a total acquisition time of 9 min 54 sec with the scan parameters TR = 5.8 ms, α = 20°, FID = 0.1 ms, LE = 5.6 ms) at a matrix size of 320³ with a resolution of 160 µm³.

The use of a balanced steady-state free precession (bSSFP) UTE sequence also allowed a reduction of acquisition time while maintaining a good contrast-to-noise ratio (CNR) (Diwoky et al., 2013).

An additional postprocessing step was then used to further emphasize the contrast of (U)SPIO particles. In brief, the acquired k-space raw data was modulated with a global frequency offset for signal recovery. Positive contrast was created by subtraction of the modulated from the unmodulated (on-resonant) image (Diwoky et al., submitted).

3 Results

3.1 Cell Labeling

Resovist®, various Molday Ion™ variants with different surface modifications (Table 2), and liposomes as transfer vehicles for each of the particles were compared for intracellular iron uptake. Cells were labeled as described in Chapter 2.4. In a first step iron uptake was visualized by Prussian Blue Staining.

3.1.1 Resovist®

As the laboratory standard, Resovist® was used to show the labeling of both MSPCs and ECFCs. Iron uptake was examined by Prussian Blue staining. Protamine sulfate was used as a cationic transfection agent (3 µg/mL). (Figure 7)

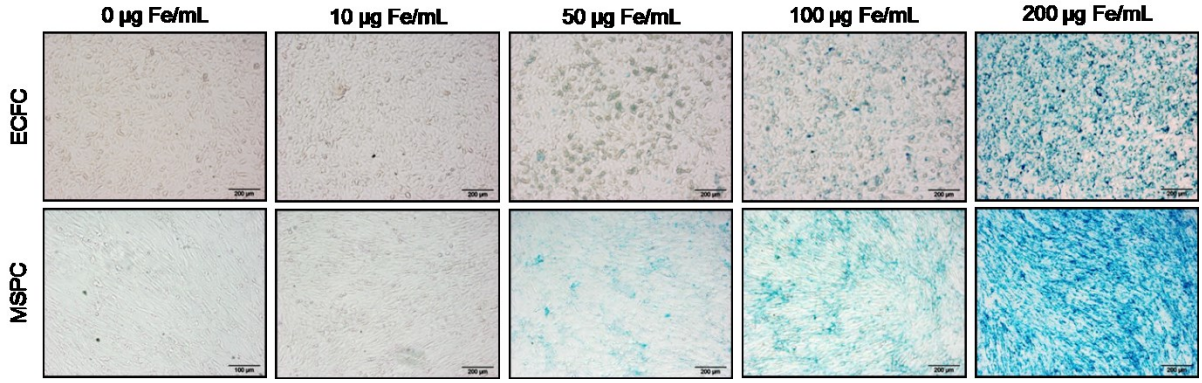

Figure 7: Representative Prussian Blue-stained MSPCs and ECFCs labeled with Resovist®. Both MSPCs and ECFCs were incubated with increasing concentrations of Resovist® (0, 10, 50, 100 and 200 µg/mL iron) all conditions with protamine sulfate (3 µg/mL). (scale bar: 200 µm).

Intracellular Iron was measured as described (Rad et al., 2007). Similar values were found as published for labeling of THP-1 and U251 cells with 50 and 100 µg/mL iron. (Janic et al., 2009).

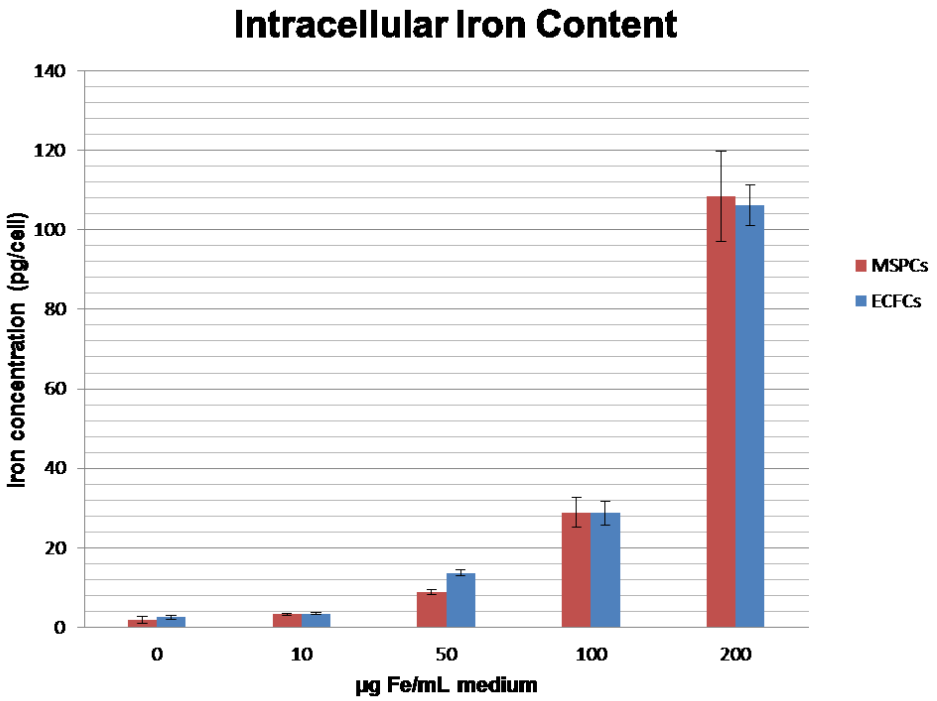

Figure 8: Intracellular iron concentration of both MSPCs and ECFCs. Cells were labeled with 10, 50, 100 and 200 µg/mL of iron and 3 µg/mL protamine sulfate. Data expressed as means values including standard deviations.

3.1.2 Liposomes as Transfection agents

An approach to incorporate Molday Ion™ or Resovist® into ECFCs was to utilize POPC liposomes as delivery agents. Two different fluorophores, FITC and ATTO 655, and unmodified and PEGylated liposomes were tested. As can be seen in Figure 9, the best liposomal visualization was achieved with FITC-conjugated liposomes. Flow cytometry showed no difference in cellular uptake between PEG-ylated and unmodified FITC-conjugated liposomes.

Intracellular liposome localisation is demonstrated as superposition of red plasma membrane stain and green FITC-labeled liposomes. In contrast, incorporation of ATTO655 conjugated liposome could not be shown with fluorescence microscopy.

Further liposome experiments were therefore performed with FITC-conjugated, surface-unmodified liposomes. To test, wether they are capable of transfering (U)SPIO contrast agents into a cell, ECFCs were incubated with different concentrations of either Molday Ion™- or Resovist®-containing liposomes and were compared to ECFCs. These control cells were unmodified or labeled with Molday Ion™ or Resovist® only (Figure 10). While ECFCs incubated with Resovist®-containing Liposomes appeared

as Prussian Blue positive, Molday Ion™-containing Liposomes showed no intracellular localized iron.

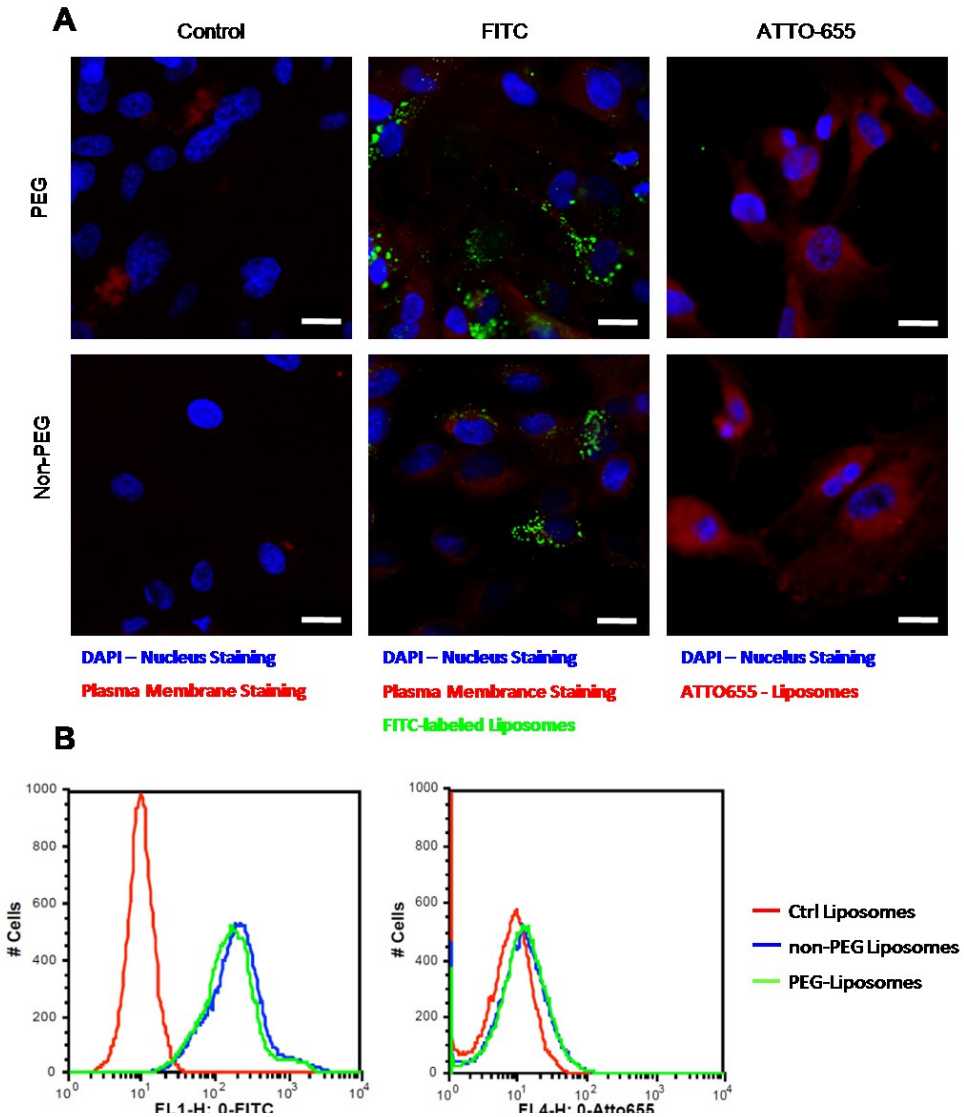

Figure 9: Different fluorophores were tested for liposome visualization. A: Control cells were labeled with diamidino-phenylindole (DAPI) and Plasma Membrane Stain after overnight incubation with 500 µg/mL Liposomes. Fluorescein isothiocyanate (FITC)- and ATTO 655-conjugated liposomes where tested for intracellular localization with either unmodified (non-PEG) or PEG-ylated surface (white scale bar: 20 µm). **B**: Flow cytometry histograms of 10 000 ECFCs, either treated with FITC- or ATTO 655- conjugated liposomes.

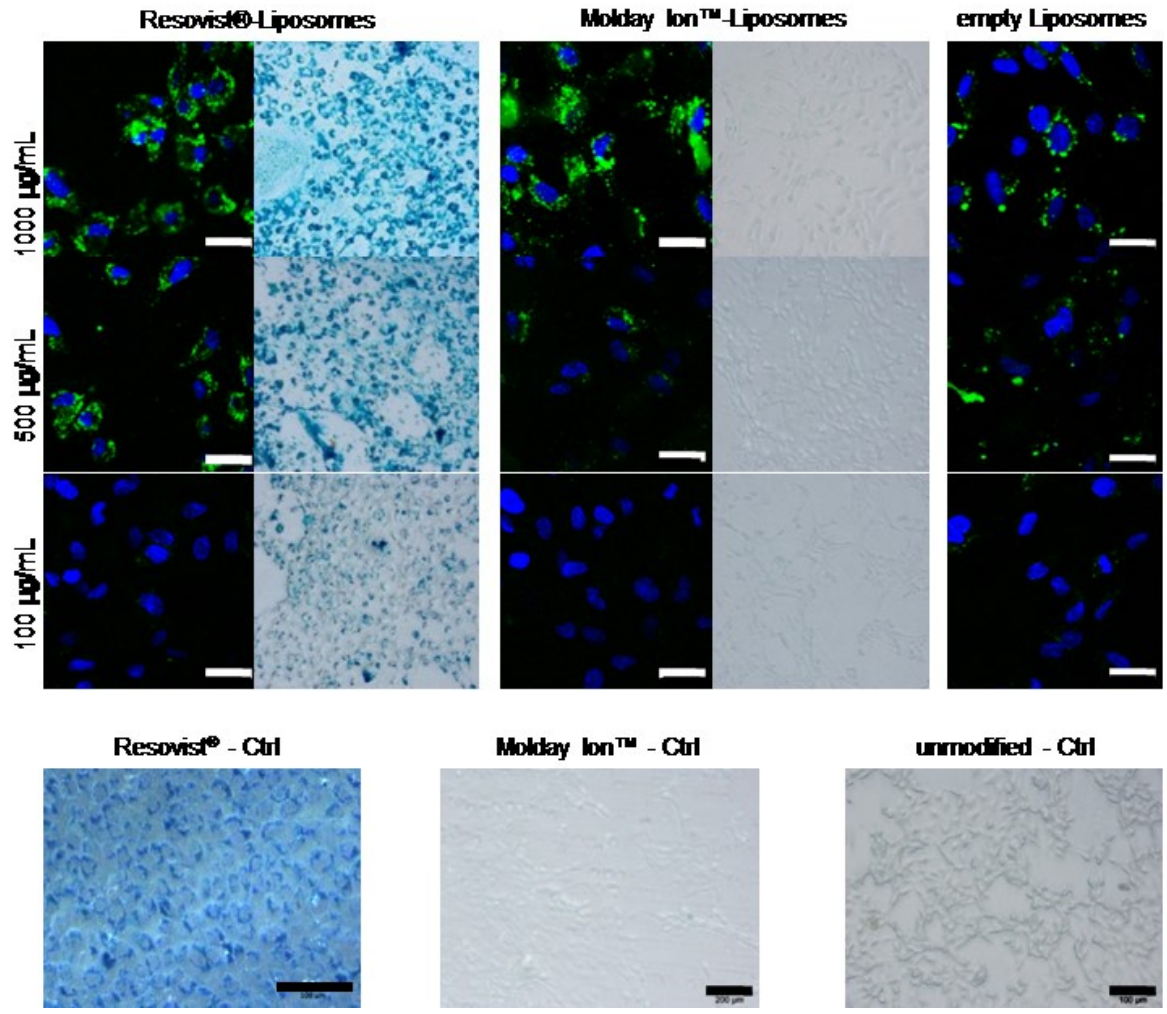

Figure 10: Comparison of different (U)SPIO-containing liposomes as labeling vehicle. Fluorescence microscopy images of FITC-conjugated, iron-containing liposomes were counterstained with DAPI (white scale bar: 20 µm). ECFCs were incubated with increasing concentrations of liposomes (100, 500 and 1000 µg/mL), and overview images of Prussian Blue stained cell culture were taken. Only Resovist-Liposomes showed an uptake of iron, similar to Resovist® control cells.

3.1.3 Molday Ion™

USPIOs like Molday Ion™ provide a R1/R2 ratio next to 1. This enables a higher signal from short T2 species in combination with ultrashort imaging sequences compared to larger SPIO particles like Resovist® with a R2 relaxivity usually one order of magnitude greater than R1 (see Table 2) due to the size of its iron core.

3.1.3.1 Molday Ion™ manufacturer protocol

In a first experiment Molday Ion™ was tested for its uptake in ECFCs. Cells were grown to 90% confluence, labeled as given by the manufacturer's instructions (BioPAL, 2013) and subsequently stained with Prussian Blue as described above.

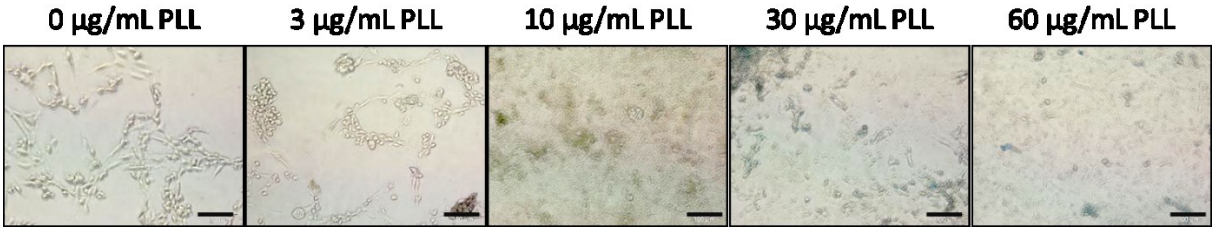

Figure 11: Endothelial Colony Forming Cells (ECFC) labeling with Molday Ion™. Umbilical cord-derived ECFCs were labeled with Molday Ion™ (50 µg iron/mL) and different concentrations of poly-L-lysine (PLL). Cells were already partially detached prior labeling with Prussian Blue. An iron-containing superimposing layer was rinsed off during staining. Intracellular iron uptake could not be determined. (scale bar: 100µm)

A visual inspection prior to staining revealed detached, senescent cells. During washing and labeling steps cells, and an overlying unidentified layer, were mostly rinsed away (Figure 11).

3.1.3.2 Molday Ion™ concentration series

To test different possible working conditions for Molday Ion™ species the labeling protocol was adapted. RPMI-1640 was used for the labeling solution instead of distilled water to preserve osmolality of culture medium. Three different Molday Ion™ variants with either neutral (Figure 12), positive (Figure 13) or negative surface charge (Figure 14) were examined. Different concentrations for both the USPIO and the transfection agents were tested. These concentration series showed a similar result. Cells were

unable to incorporate USPIOs and detached partially. Again a similar overlying iron-positive layer could be seen, which again could be rinsed off the cells.

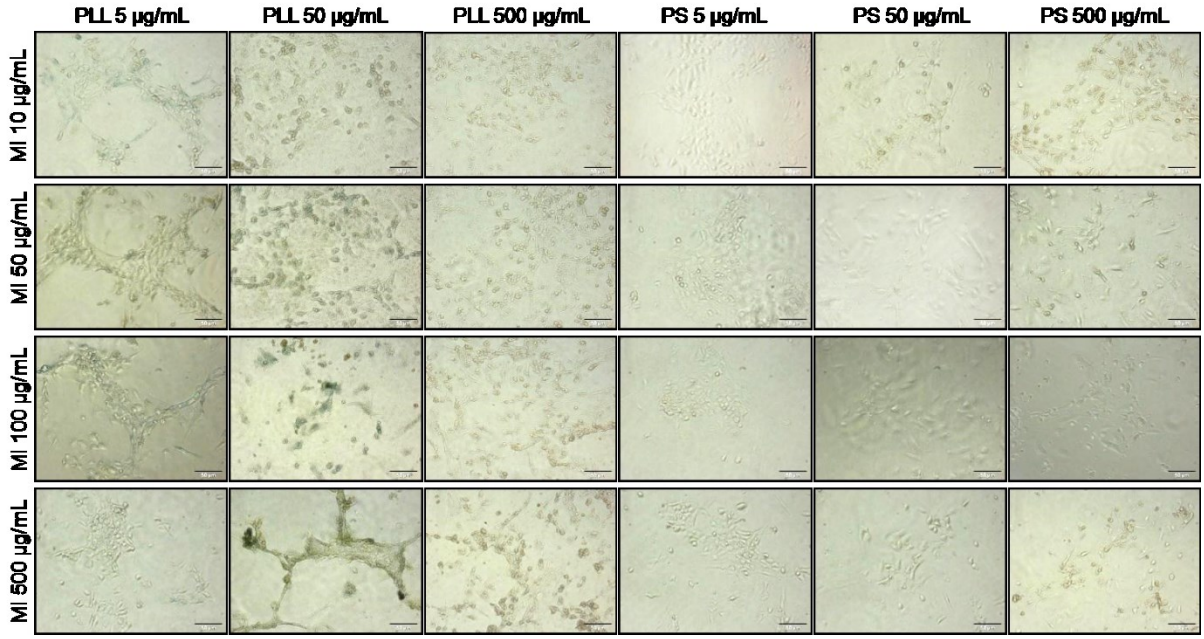

Figure 12: Molday Ion™ (MI, with neutral surface charge) concentration series. Umbilical cord-derived ECFCs were labeled with Molday Ion® and different concentrations of poly-L-lysine (PLL). Cells were already partially detached prior to labeling with Prussian Blue. An iron-containing superimposing layer was rinsed off during staining. Intracellular iron uptake could not be determined. (scale bar: 100 µm)

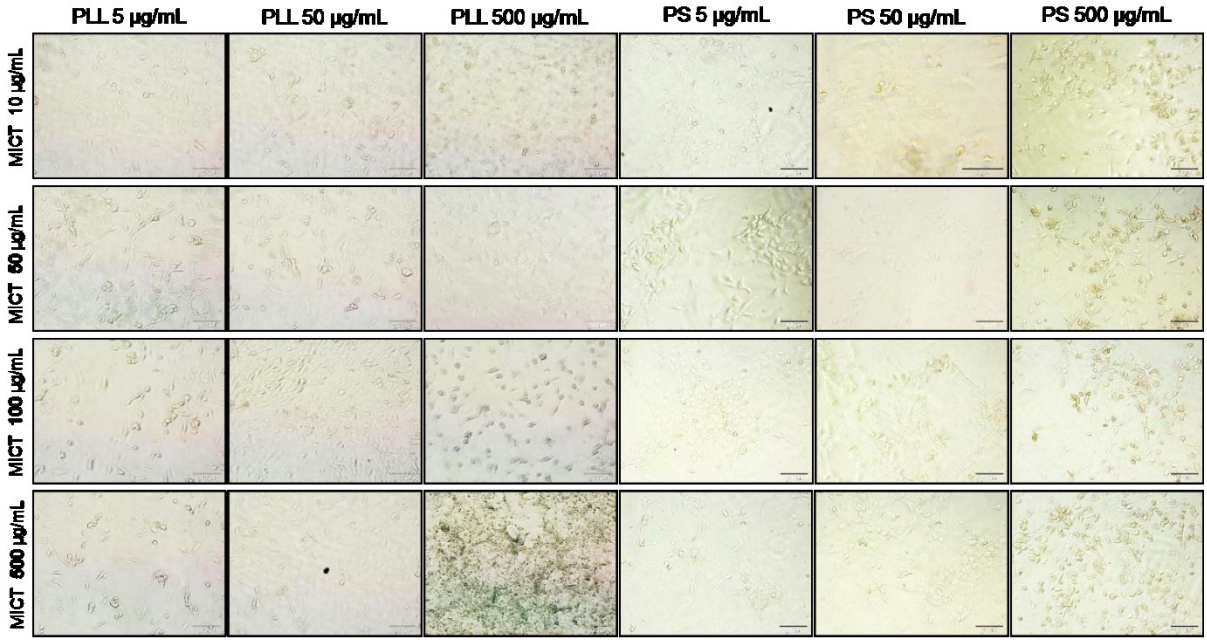

Figure 13: Molday Ion™ CT (MICT, with positive surface charge) concentration series. Umbilical cord-derived ECFCs were labeled with Molday Ion® and different concentrations of poly-L-lysine (PLL). Cells were already partially detached prior to labeling with Prussian Blue. An iron-containing superimposing layer was rinsed off during staining. Intracellular iron uptake could not be determined. (scale bar: 100 µm)

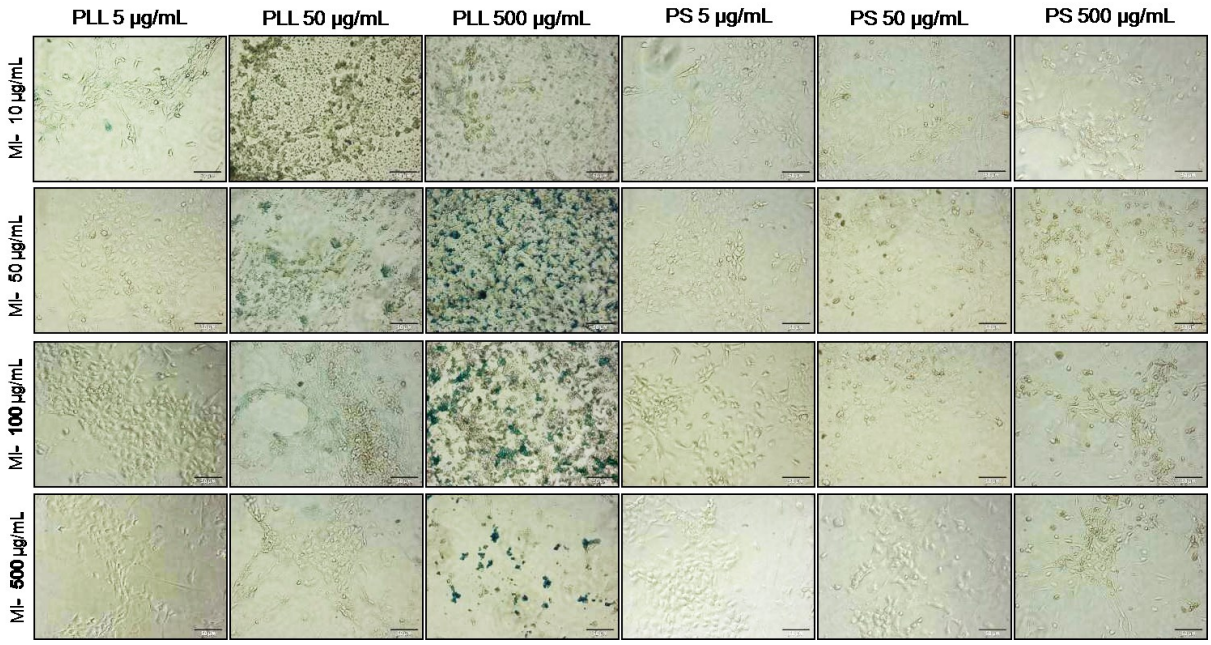

Figure 14: Molday Ion™ (-) (negative surface charge) concentration series. Umbilical cord-derived ECFCs were labeled with Molday Ion™ (-) and different concentrations of poly-L-lysine PLL). Cells were partially detached prior to labeling with Prussian Blue. An iron-containing superimposing layer was partially rinsed off during staining. Remaining parts of this layer can be seen in the images with 500

µg/mL PLL and 50, 100 and 500 µg/mL MI-. Intracellular iron uptake could not be determined. (scale bar: 100 µm)

3.2 Cellular Function

3.2.1 MSPC

MSPC differentiation potential for adipogenic, osteogenic and chondrogenic lineage was subsequently examined after labeling as described above. MSPCs showed iron concentration independent differentiation capacity as can be seen in Figure 15.

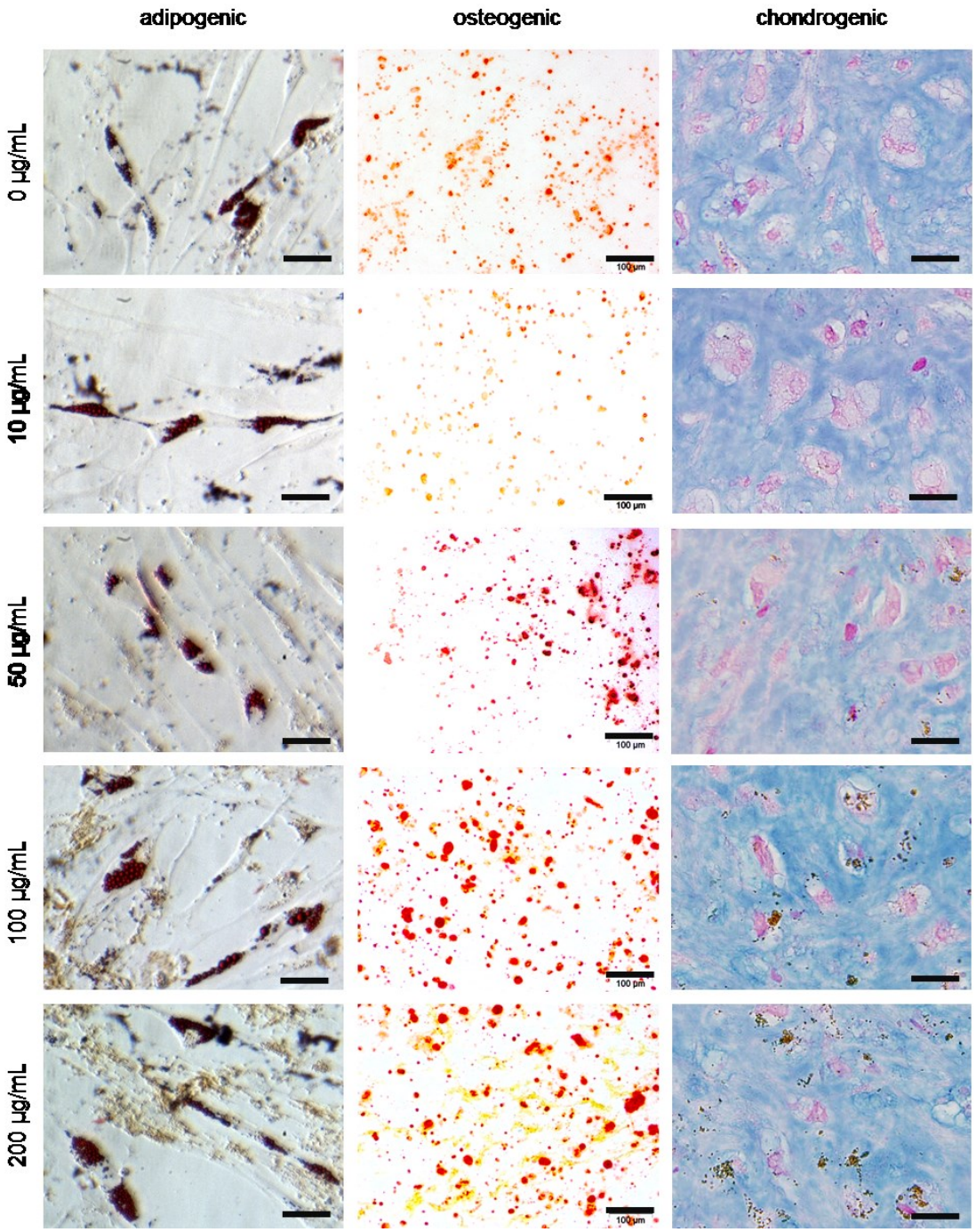

Figure 15: MSPCs differentiation capacity after labeling with Resovist®. Intracellular iron can be seen as yellow to brownish coloration within the outlined cells. **Adipogenic differentiation:** Accumulation of lipid vacuoles can be seen as collection of prominent round dark red bubbles (Oil Red O staining, scalebar: 50µm). **Osteogenic differentiation**: Red dots indicate calcium depositions (Alkaline Phosphatase staining, scalebar: 100µm). **Chondrogenic differentiation**: Glycosaminoglycans appear as blue background (Alcian Blue staining, scale bar: 25µm).

3.2.2 ECFC

The network formation experiment was performed and data kindly provided by Dr. Andreas Reinisch, PhD.

An *in vitro* model of vascular network formation using Matrigel® was utilized to test functionality of ECFCs labeled with high doses of SPIOs. Both conditions presented complex vascular network formation. Using Computer-assisted image assembling, network propagation over the entire culture area could be observed. By using time lapse video-microscopy, network formation was found to have resulted from ECFC migration and morphogenesis rather than proliferation (Reinisch et al., 2009).

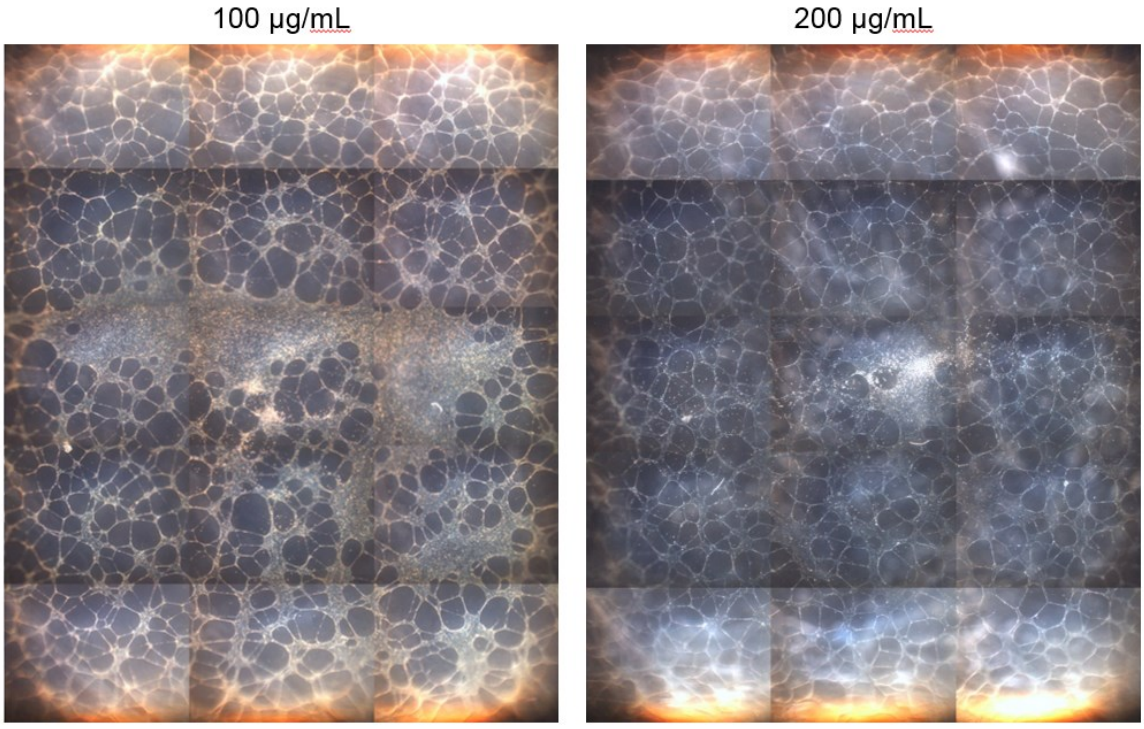

Figure 16: ECFCs function *in vitro* after high dose iron labeling. Assembled images show network structures of Resovist®-labeled ECFCs visualized by dark field microscopy

3.2.3 Tracking labeled cells with MR

MRI is considered as one of the major techniques when it comes to the evaluation of the functional effects of cellular therapy. One key question, which has to be addressed is the fate of stem cells after transplantation. A desirable application of MRI would be the tracking of labeled stem cells within days after transplantation. Therefore it is necessary to provide high resolution combined with both high sensitivity and specificity.

The detection limit of labeled cells can be decreased in several ways when using MRI. At cellular level this can be achieved by choosing a contrast agent with high relaxivity values and by increasing the iron load per cell. On the technical side several other approaches to gain sensitivity and specificity can be used. This includes the selection of appropriate imaging devices and coils, the development of customized sequences and the use of optimized postprocessing steps.

An agarose-containing phantom was used to test the feasibility of the developed MRI sequences for cellular imaging on a clinical 3 Tesla MRI scanner. Agarose was admixed with Gadolinium–DTPA and Resovist to reach human muscle comparable magnetic properties. (T1/T2 = 1074/65.9 ms).

3.2.4 Targeting labeled cells *in vivo*

To analyze the signal behavior of labeled cells in vivo, a model for vessel formation in immune-deficient mice was utilized to provide a relatively homogenous background for imaging. Two million cells, both MSPCs and ECFCs were mixed at a ratio of 20:80 in Matrigel®. Either 0, 400, 2000 or 10000 Resovist®-labeled ECFCs were admixed and injected into the flanks of a mouse as described above. Imaging was performed at different time points.

Imaging with a UTE sequence did not show major changes of mean voxel values for 400 and 2000 labeled cells while perturbances of the local magnetic field by SPIO labeling of 10000 cells can be seen clearly.

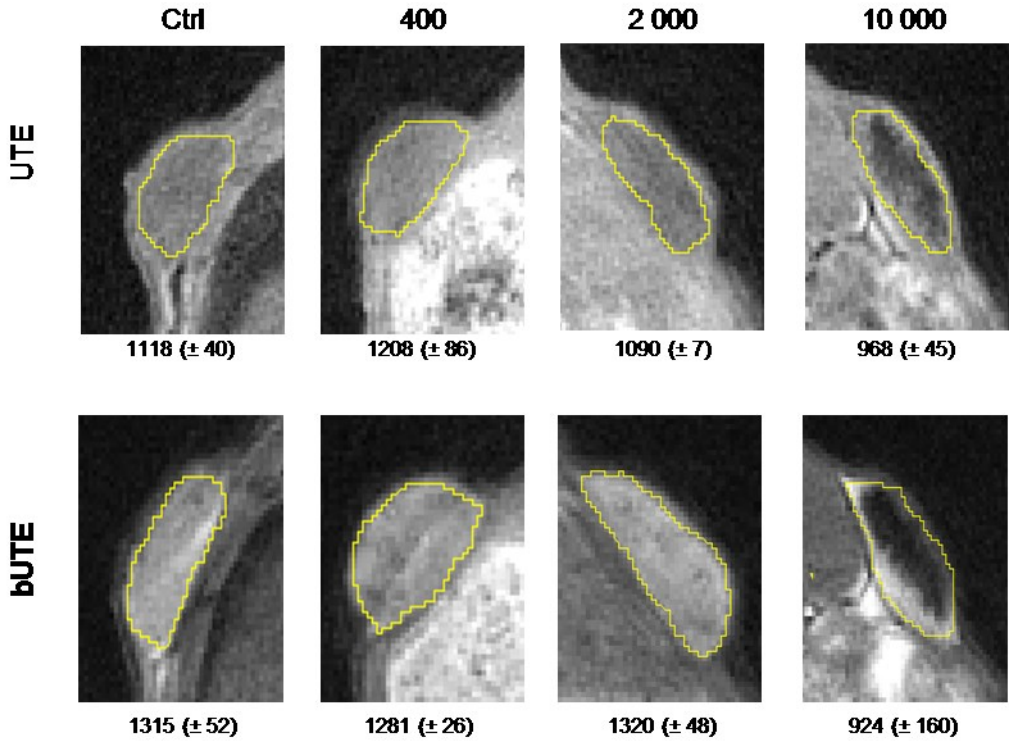

Figure 17: Injected plugs were imaged at day 14 with two different ultrashort time of echo sequences. The images shows a representative slice of each plug consisting of 2 million unlabeled cells and with either none, 400, 2000 or 10000 Resovist® labeled cells admixed in Matrigel®. The number below each image shows the mean pixel value (± SD) of the yellow bordered area. Arrows point to artifacts resulting from local magnetic field inhomogeneities.

Utilizing a bUTE sequence permitted the recognition of local magnetic field inhomogeneities generated by 400 labeled cells as can be seen by dark rings within the bright plug background (Figure 17). Assuming a total injected plug volume of 200 µL, and voxel volume of 8.192×10^{-3} µL (160 µm × 160 µm × 320 µm) this results in 0.016 labeled cells per voxel or 1 cell in every sixty-first voxel. The marked area represents 452 voxels therefore approximately 7 labeled cells are within the image. At least 4 artifacts, produced by labeled cells (white arrows, Figure 17) can be seen. This artifacts appear as annular darkenings with a lighter center and were already simulated (Diwoky et al., 2013)

3.3 Optimization

Optimization and MRI sequence development was performed by DI Clemens Diwoky.

Sensitivity of MRI can be increased by optimizing imaging sequences and adaptation according to the structures to be imaged. Considering the properties of imaging contrast agents, further enhancement can be done (Figure 18 and Figure 19) to highlight labeled cells.

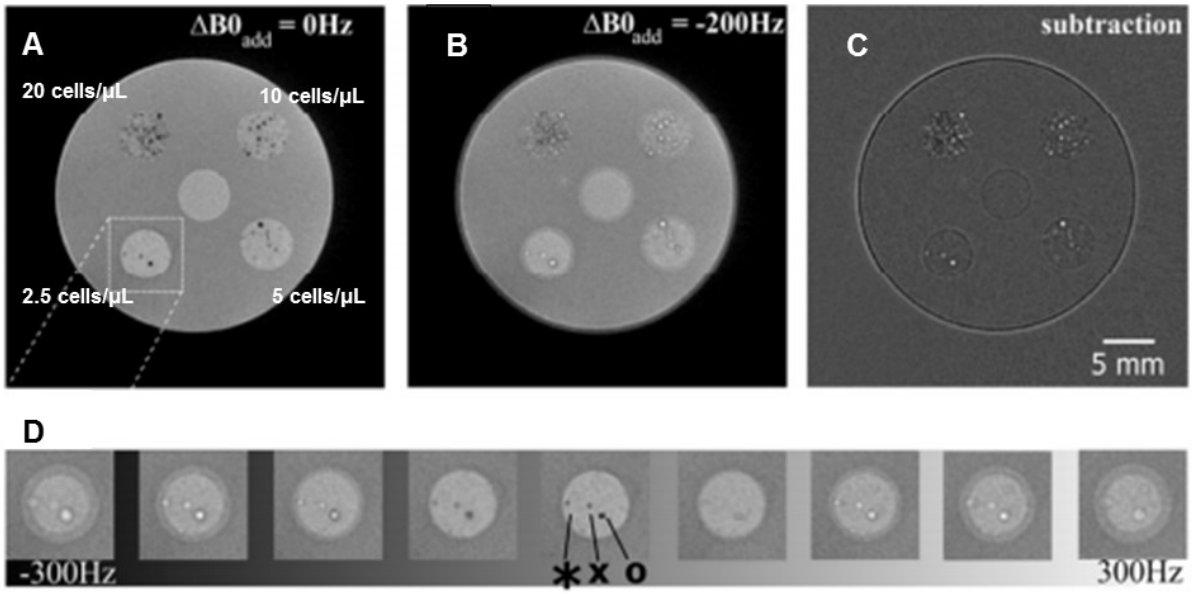

Figure 18: Postprocessing for further enhancement of signal specifity *in vitro*. ECFCs were filled into cavities of an agarose phantom. The central cavity contains 20 unlabeled cells/µL. The outer cavities comprise Resovist®-labeled ECFCs in a concentration of 2.5, 5, 10 and 20 cells/µL (starting from the lower left, counterclockwise). **A**: Standard bUTE image without any postproccessing modification. **B:** A Frequency offset (ΔB_{0add}) of -200 Hz was added to the raw data before reconstruction. **C**: The subtraction of image A and B results in an image with accentuated positive contrast of labeled ECFCs. D: Reconstruction with values for ΔB_{0add} ranging from -300 to +300 Hz shows the signal alteration inherent to labeled cells.

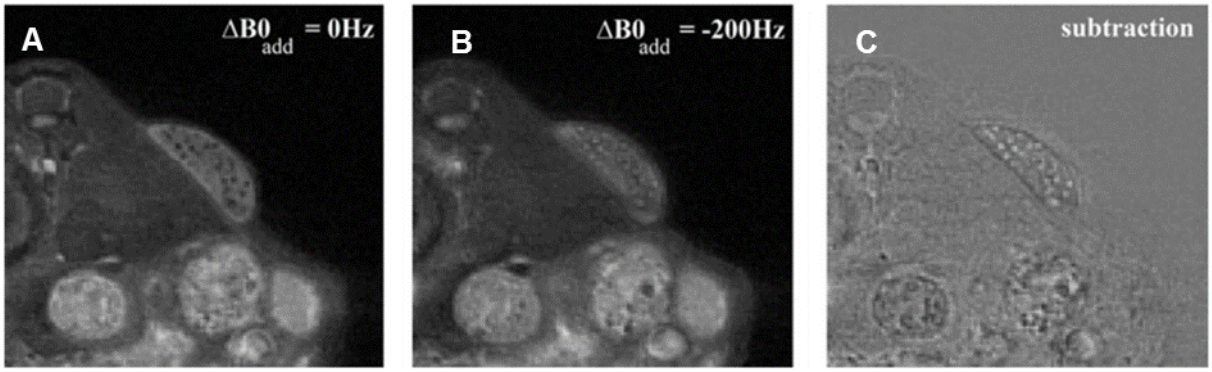

Figure 19: Postprocessing for further enhancement of specifity *in vivo*. 2x10^6 MSPC and ECFC (20:80) in Matrigel® were admixed with 2000 labeled ECFCs. A bUTE sequence was utilized for imaging at day 14 after implantation of the plug. **A:** The unmodified raw data without the addition of a frequency offset after reconstruction. **B**: A frequency offset of -200 Hz was added prior to reconstruction. **C**: A subtraction image of A and B is calculated.

4 Discussion

Although stem cell tracking has become a heavily investigated topic since the beginning of regenerative medicine, there is still an obvious lack of sufficient *in vivo* technology. Many questions have been raised regarding optimal imaging modality, contrast agent, labeling and application procedure. This work focused on MRI because of its good spatial resolution when used with small animal models in combination with vast possibilities for modification and optimization.

The rationale for the investigation of Molday Ion™ was the supposed contrast enhancement due to higher relaxivity values than the gold standard Resovist®. Different Molday Ion™ species have already been reported to provide good labeling efficiency for MSPCs of different origin without a negative impact on proliferation and differentiation (Addicott et al., 2011; Barczewska et al., 2013; Jülke et al., 2013). It was not possible to reproduce an intracellular uptake of Molday Ion™ or its surface-modified equivalents Molday Ion™ CT and Molday Ion™(-). An examination of (U)SPIO-containing liposomes for labeling purposes showed no uptake of Molday Ion™ particles.

Further cell labeling was therefore performed with Resovist®. Differentiation in adipogenic, osteogenic and chondrogenic lineage for MSPCs and network formation for ECFCs was not impaired after labeling with high doses of SPIO. A spectrometric method was established to measure the intracellular iron content and revealed similar values of iron per cell for both ECFCs and MSCs as compared to others (Rad et al., 2007).

A bSSFP imaging regimen was used for in vitro and in vivo imaging. As already pointed out, the advantage of this approach is its high SNR efficiency, allowing for imaging at high resolutions within reasonable MRI data acquisition times and its high sensitivity to magnetic field disturbers like (U)SPIO contrast agents. An annular artifact was found during imaging and its origin from SPIO-labeled cells was successfully simulated by colleagues of the Institute of Medical Engineering, Technical University of Graz. An postprocessing step was added to emphasize this artifact as positive imaging contrast (Diwoky et al., 2013 submitted). The utilization of this technique made it possible to reach a nearly single cell detection limit within the implanted plug.

Although this imaging approach shows promising results for non-invasive small animal imaging, several drawbacks have to be mentioned. In consequence of the small voxel size, the FOV is limited to several centimeters with current MRI scanners due to technical limitations thus making this technique exclusively applicable for small animal models. Single cell detection is further restricted to tissues or experimental models providing a homogenous background signal. Another disadvantage, generally attributed to directly labeled cell tracking approaches, is the inability to distinguish between living labeled cells and iron-containing cellular debris. To solve this problems by MRI different approaches can be used:

An increased specifity, can be reached by the use of chemical exchange saturation transfer CEST contrast mechanism. This technique makes use of the different resonance frequencies of protons associated with a molecule (the CEST agent) and the surrounding water. The associated proton can be saturated by a RF pulse therefore creating a switchable contrast behavior (Vinogradov et al., 2012).

Another promising technique to increase MR specifity is the use of “second color” or “hot-spot” imaging with ^{13}C, ^{23}Na, ^{31}P or ^{19}F. Fluorinated (^{19}F) labels for MRI are the most promising ones due to the low occurrence of this element with the body. Proton (^{1}H) based MRI contrast agents function by modifying the contrast of images by altering the local magnetic field homogeneity thus making unambiguous localization difficult. The use of fluorinated labels enables direct detection thus greatly enhancing specifity (Ahrens and Zhong, 2013; Srinivas et al., 2010).

Sensitivity can be increased by utilization of ultra-high field MRI devices (17.6 T) although this work can only be done in highly specialized centers and is therefore unsuitable for most preclinical experiments (Bengtsson et al., 2011).

Iron oxide-based contrast agents were commonly used in many investigations in the last decade and labeling protocols were optimized for greater sensitivity (Arbab et al., 2004, 2005; Janic et al., 2009; Liu and Frank, 2009; Rad et al., 2007). They have also been an important field for investigation itself to maximize relaxivity values per cell (Gossuin et al., 2009; Marco et al., 2007; Vetter et al., 2011).

The discrimination of living and dead iron-labeled cells by MRI is feasible to some extent with a bSSFP sequence (Ribot and Foster, 2012) although a better investigated and more elegant solution for this distinction will be the use of reporter genes which are degraded after cell death.

Many of the MRI techniques are currently investigated for their feasibility but are hardly integrable with each other due to complex sequence design. But besides this a lot of other imaging modalities are available. To overcome the disadvantages of a single modality, techniques should be combined to get a maximum benefit.

While specifity and sensitivity can be increased by using PET or SPECT scanners, a combined imaging with CT allows an appropriate anatomic representation of the studied object. This modalities also enable the utilization of larger animal models or even the examination of human individuals.

As with MRI direct labeling agents it is necessary to address the question of imaging a living cell or just the remaining cell label. As pointed out and demonstrated by Lassailly and colleagues it is crucial to cross validate results by using multi-modality approaches when using non-genetically encoded cell markers (Lassailly et al., 2010, 2013). By using a genetically modified target cell it is possible to successfully track living cells over a time period of up to 15 weeks as shown by Templin et al. in a myocardial infarction model in pig. This is achieved by using a transgenic human-induced pluripotent stem cell expressing both a fluorescent reporter for histologic analysis and an iodide transporter to accumulate ^{123}I after its intracoronary administration for tracking over time. The use of a radionuclide with a half-time of approximately 13 hours and its accumulation within the tracked cells is furthermore an elegant way to circumvent the problem of retained accumulation after cell death of non-decaying cellular labels (Templin et al., 2012).

The use of MRI for cellular tracking requires a close coordination of both biomedical and imaging aspects. Result quality strongly depends on a joint approach with well-known parameters starting from the experimental model influencing the coil and MRI setup up to e.g. cellular iron load which affects the MRI sequence parameters.

The imaging approach used in this thesis utilized specialized sequences to gain resolution and sensitivity as well as postprocessing steps for increased specifity. It was possible to reach a remarkable, nearly single cell detection limit within a limited volume with a standard 3T clinical MRI scanner. Further adaptation of this imaging approach will allow addressing topics like bio-distribution and availability as well as homing behavior of cells, thus supporting the clinical research in cellular therapy as well as in regenerative medicine.

5 References

Addicott, B., Willman, M., Rodriguez, J., Padgett, K., Han, D., Berman, D., Hare, J.M., and Kenyon, N.S. (2011). Mesenchymal stem cell labeling and in vitro MR characterization at 1.5 T of new SPIO contrast agent: Molday ION Rhodamine-B^{TM}. Contrast Media Mol. Imaging *6*, 7–18.

Ahrens, E.T., and Zhong, J. (2013). *In vivo* MRI cell tracking using perfluorocarbon probes and fluorine-19 detection: *In Vivo Cell Tracking Using* ^{19}F MRI. NMR Biomed. *26*, 860–871.

Allan, D.S., and Strunk, Dirk (2012). Regenerative Therapy Using Blood-Derived Stem Cells (Humana Press).

Arbab, A.S., Yocum, G.T., Wilson, L.B., Parwana, A., Jordan, E.K., Kalish, H., and Frank, J.A. (2004). Comparison of transfection agents in forming complexes with ferumoxides, cell labeling efficiency, and cellular viability. Mol. Imaging *3*, 24–32.

Arbab, A.S., Yocum, G.T., Rad, A.M., Khakoo, A.Y., Fellowes, V., Read, E.J., and Frank, J.A. (2005). Labeling of cells with ferumoxides-protamine sulfate complexes does not inhibit function or differentiation capacity of hematopoietic or mesenchymal stem cells. NMR Biomed. *18*, 553–559.

Barczewska, M., Wojtkiewicz, J., Habich, A., Janowski, M., Adamiak, Z., Holak, P., Matyjasik, H., Bulte, J.W.M., Maksymowicz, W., and Walczak, P. (2013). MR Monitoring of Minimally Invasive Delivery of Mesenchymal Stem Cells into the Porcine Intervertebral Disc. PLoS ONE *8*, e74658.

Barnes, D.W., Corp, M.J., Loutit, J.F., and Neal, F.E. (1956). Treatment of murine leukaemia with X rays and homologous bone marrow; preliminary communication. Br. Med. J. *2*, 626–627.

Bartmann, C., Rohde, E., Schallmoser, K., Pürstner, P., Lanzer, G., Linkesch, W., and Strunk, D. (2007). Two steps to functional mesenchymal stromal cells for clinical application. Transfusion (Paris) *47*, 1426–1435.

Battiwalla, M., and Hematti, P. (2009). Mesenchymal stem cells in hematopoietic stem cell transplantation. Cytotherapy *11*, 503–515.

Bengtsson, N. E., Kim, S., Lin, L., Walter, G.A., and Scott, E.W. (2011). Ultra-high-field MRI real-time imaging of HSC engraftment of the bone marrow niche. Leukemia *25*, 1223–1231.

Bianco, P. (2011). Bone and the hematopoietic niche: a tale of two stem cells. Blood *117*, 5281–5288.

Bianco, P., Robey, P.G., and Simmons, P.J. (2008). Mesenchymal stem cells: revisiting history, concepts, and assays. Cell Stem Cell *2*, 313–319.

Biglands, J.D., Radjenovic, A., and Ridgway, J.P. (2012). Cardiovascular magnetic resonance physics for clinicians: part II. J. Cardiovasc. Magn. Reson. *14*, 66.

BioPAL (2013). Protocol for Cell Labeling with CL-30Q02-6 Treated with Polylysine.

Le Blanc, K., Rasmusson, I., Sundberg, B., Götherström, C., Hassan, M., Uzunel, M., and Ringdén, O. (2004). Treatment of severe acute graft-versus-host disease with third party haploidentical mesenchymal stem cells. Lancet *363*, 1439–1441.

Bulte, J.W.M., and Kraitchman, D.L. (2004). Iron oxide MR contrast agents for molecular and cellular imaging. NMR Biomed. *17*, 484–499.

Bydder, G.M. (2011). Review. The Agfa Mayneord lecture: MRI of short and ultrashort T_2 and T_2* components of tissues, fluids and materials using clinical systems. Br. J. Radiol. *84*, 1067–1082.

Cromer Berman, S.M., Kshitiz, Wang, C.J., Orukari, I., Levchenko, A., Bulte, J.W.M., and Walczak, P. (2013). Cell motility of neural stem cells is reduced after SPIO-labeling, which is mitigated after exocytosis. Magn. Reson. Med. *69*, 255–262.

Diwoky, C., Gungl, D., Reinisch, A., Hofmann, N.A., Strunk, D., and Stollberger, R. (2013). Off-Resonant Reconstruction of Balanced 3D-Radial Acquisitions with Half-Echo Sampling for Unique Cell Tracking Contrast. In International Society for Magnetic Resonance in Medicine: Scientific Meeting & Exhibition 2013, (Salt Lake City), p. 765.

Dominici, M., Le Blanc, K., Mueller, I., Slaper-Cortenbach, I., Marini, F., Krause, D., Deans, R., Keating, A., Prockop, D., and Horwitz, E. (2006). Minimal criteria for defining multipotent mesenchymal stromal cells. The International Society for Cellular Therapy position statement. Cytotherapy *8*, 315–317.

Ernest, G. (2011). Relaxation values for BioPAL products (Worcester and MA).

Farrell, E., Wielopolski, P., Pavljasevic, P., van Tiel, S., Jahr, H., Verhaar, J., Weinans, H., Krestin, G., O'Brien, F.J., van Osch, G., et al. (2008). Effects of iron oxide incorporation for long term cell tracking on MSC differentiation in vitro and in vivo. Biochem. Biophys. Res. Commun. *369*, 1076–1081.

Gerlinde Schmidtke-Schrezenmeier, Urban, M., Musyanovych, A., Mailänder, V., Rojewski, M., Fekete, N., Menard, C., Deak, E., Tarte, K., Rasche, V., et al. (2011). Labeling of mesenchymal stromal cells with iron oxide–poly(l-lactide) nanoparticles for magnetic resonance imaging: uptake, persistence, effects on cellular function and magnetic resonance imaging properties. Cytotherapy *13*, 962–975.

Gonzalez-Lara, L.E., Xu, X., Hofstetrova, K., Pniak, A., Chen, Y., McFadden, C.D., Martinez-Santiesteban, F.M., Rutt, B.K., Brown, A., and Foster, P.J. (2010). The Use of Cellular Magnetic Resonance Imaging to Track the Fate of Iron-Labeled Multipotent Stromal Cells after Direct Transplantation in a Mouse Model of Spinal Cord Injury. Mol. Imaging Biol. *13*, 702–711.

Gossuin, Y., Gillis, P., Hocq, A., Vuong, Q.L., and Roch, A. (2009). Magnetic resonance relaxation properties of superparamagnetic particles. Wiley Interdiscip. Rev. Nanomed. Nanobiotechnol. *1*, 299–310.

Hao, D., Ai, T., Goerner, F., Hu, X., Runge, V.M., and Tweedle, M. (2012). MRI contrast agents: Basic chemistry and safety. J. Magn. Reson. Imaging *36*, 1060–1071.

Horwitz, E.M., Prockop, D.J., Gordon, P.L., Koo, W.W., Fitzpatrick, L.A., Neel, M.D., McCarville, M.E., Orchard, P.J., Pyeritz, R.E., and Brenner, M.K. (2001). Clinical responses to bone marrow transplantation in children with severe osteogenesis imperfecta. Blood *97*, 1227–1231.

Jacques, V., Dumas, S., Sun, W.-C., Troughton, J.S., Greenfield, M.T., and Caravan, P. (2010). High relaxivity MRI contrast agents part 2: Optimization of inner- and second-sphere relaxivity. Invest. Radiol. *45*, 613–624.

Janic, B., Rad, A.M., Jordan, E.K., Iskander, A.S.., Ali, M.M., Varma, N.R.S., Frank, J.A., Arbab, A.S., and Yang, S. (2009). Optimization and Validation of FePro Cell Labeling Method. PLoS ONE *4*, e5873.

Jiao, Y., Peng, Z.-H., Zhang, J.-Y., Qin, J., and Zhong, C.-P. (2008). Liposome-Mediated Transfer Can Improve the Efficacy of Islet Labeling With Superparamagnetic Iron Oxide. Transplant. Proc. *40*, 3615–3618.

Jülke, H., Veit, C., Ribitsch, I., Brehm, W., Ludewig, E., and Delling, U. (2013). Comparative labelling of equine and ovine multipotent stromal cells with superparamagnetic iron oxide particles for magnetic resonance imaging in vitro. Cell Transplant.

Kircher, M.F., Gambhir, S.S., and Grimm, J. (2011). Noninvasive cell-tracking methods. Nat. Rev. Clin. Oncol. *8*, 677–688.

Kraitchman, D.L., and Caravan, P. (2009). Magnetic Resonance Labeling of Stem Cells. JACC Cardiovasc. Imaging *2*, 1123–1125.

Lassailly, F., Griessinger, E., and Bonnet, D. (2010). Microenvironmental contaminations induced by fluorescent lipophilic dyes used for noninvasive in vitro and in vivo cell tracking. Blood *115*, 5347–5354.

Lassailly, F., Foster, K., Lopez-Onieva, L., Currie, E., and Bonnet, D. (2013). Multimodal imaging reveals structural and functional heterogeneity in different bone marrow compartments: functional implications on hematopoietic stem cells. Blood *122*, 1730–1740.

Mani, V., Adler, E., Briley-Saebo, K.C., Bystrup, A., Fuster, V., Keller, G., and Fayad, Z.A. (2008). Serial in vivo positive contrast MRI of iron oxide-labeled embryonic stem cell-derived cardiac precursor cells in a mouse model of myocardial infarction. Magn. Reson. Med. *60*, 73–81.

Marco, M.D., Sadun, C., Port, M., Guilbert, I., Couvreur, P., and Dubernet, C. (2007). Physicochemical characterization of ultrasmall superparamagnetic iron oxide particles (USPIO) for biomedical application as MRI contrast agents. Int. J. Nanomedicine *2*, 609.

Mukherjee, S., and Thrasher, A.J. (2013). Gene therapy for PIDs: Progress, pitfalls and prospects. Gene *525*, 174–181.

Nauta, A.J., and Fibbe, W.E. (2007). Immunomodulatory properties of mesenchymal stromal cells. Blood *110*, 3499–3506.

Otsuru, S., Gordon, P.L., Shimono, K., Jethva, R., Marino, R., Phillips, C.L., Hofmann, T.J., Veronesi, E., Dominici, M., Iwamoto, M., et al. (2012). Transplanted bone marrow mononuclear cells and MSCs impart clinical benefit to children with osteogenesis imperfecta through different mechanisms. Blood.

Phinney, D.G., and Prockop, D.J. (2007). Concise Review: Mesenchymal Stem/Multipotent Stromal Cells: The State of Transdifferentiation and Modes of Tissue Repair-Current Views. Stem Cells *25*, 2896–2902.

Prassl, R., Frascione, D., Diwoky, C., Almer, G., Opriessnig, P., Vonach, C., Gradauer, K., Leitinger, G., Mangge, H., and Stollberger, R. (2012). Ultrasmall superparamagnetic iron oxide (USPIO)-based liposomes as magnetic resonance imaging probes. Int. J. Nanomedicine 2349.

Prockop, D.J. (2007). Stemness does not explain the repair of many tissues by mesenchymal stem/multipotent stromal cells (MSCs). Clin. Pharmacol. Ther. *82*, 241–243.

Rad, A., Janic, B., Iskander, A.S. Soltanian-Zadeh, H., and Arbab, A. (2007). Measurement of quantity of iron in magnetically labeled cells: comparison among different UV/VIS spectrometric methods. BioTechniques *43*, 627–636.

Rahmim, A., and Zaidi, H. (2008). PET versus SPECT: strengths, limitations and challenges: Nucl. Med. Commun. *29*, 193–207.

Reimer, P., and Balzer, T. (2003). Ferucarbotran (Resovist): a new clinically approved RES-specific contrast agent for contrast-enhanced MRI of the liver: properties, clinical development, and applications. Eur. Radiol. *13*, 1266–1276.

Reinisch, A. (2010). PhD Thesis: Towards a better understanding of non-hematopoietic stem and progenitor cell biology and function. (Graz).

Reinisch, A., and Strunk, D. (2009). Isolation and Animal Serum Free Expansion of Human Umbilical Cord Derived Mesenchymal Stromal Cells (MSCs) and Endothelial Colony Forming Progenitor Cells (ECFCs). J. Vis. Exp.

Reinisch, A., Bartmann, C., Rohde, E., Schallmoser, K., Bjelic-Radisic, V., Lanzer, G., Linkesch, W., and Strunk, D. (2007). Humanized system to propagate cord blood-derived multipotent mesenchymal stromal cells for clinical application. Regen. Med. *2*, 371–382.

Reinisch, A., Hofmann, N.A., Obenauf, A.C., Kashofer, K., Rohde, E., Schallmoser, K., Flicker, K., Lanzer, G., Linkesch, W., Speicher, M.R., et al. (2009). Humanized large-scale expanded endothelial colony-forming cells function in vitro and in vivo. Blood *113*, 6716–6725.

Ribot, E.J., and Foster, P.J. (2012). In vivo MRI discrimination between live and lysed iron-labelled cells using balanced steady state free precession. Eur. Radiol. *22*, 2027–2034.

Ridgway, J.P. (2010). Cardiovascular magnetic resonance physics for clinicians: part I. J. Cardiovasc. Magn. Reson. *12*, 71.

Ringdén, O., Uzunel, M., Rasmusson, I., Remberger, M., Sundberg, B., Lönnies, H., Marschall, H.-U., Dlugosz, A., Szakos, A., Hassan, Z., et al. (2006). Mesenchymal stem cells for treatment of therapy-resistant graft-versus-host disease. Transplantation *81*, 1390–1397.

Rohde, E., Malischnik, C., Thaler, D., Maierhofer, T., Linkesch, W., Lanzer, G., Guelly, C., and Strunk, D. (2006). Blood monocytes mimic endothelial progenitor cells. Stem Cells Dayt. Ohio *24*, 357–367.

Rohde, E., Bartmann, C., Schallmoser, K., Reinisch, A., Lanzer, G., Linkesch, W., Guelly, C., and Strunk, D. (2007). Immune Cells Mimic the Morphology of Endothelial Progenitor Colonies In Vitro. Stem Cells *25*, 1746–1752.

Schallmoser, K., Bartmann, C., Rohde, E., Reinisch, A., Kashofer, K., Stadelmeyer, E., Drexler, C., Lanzer, G., Linkesch, W., and Strunk, D. (2007). Human platelet lysate can replace fetal bovine serum for clinical-scale expansion of functional mesenchymal stromal cells. Transfusion (Paris) *47*, 1436–1446.

Schipani, E., and Kronenberg, H.M. (2009). Adult mesenchymal stem cells. StemBook, ed. The Stem Cell Research Community. StemBook.org. doi/10.3824/stembook.1.38.1.

Srinivas, M., Heerschap, A., Ahrens, E.T., Figdor, C.G., and Vries, I.J.M. de 19F MRI for quantitative in vivo cell tracking.

Templin, C., Zweigerdt, R., Schwanke, K., Olmer, R., Ghadri, J.-R., Emmert, M.Y., Muller, E., Kuest, S.M., Cohrs, S., Schibli, R., et al. (2012). Transplantation and Tracking of Human-Induced Pluripotent Stem Cells in a Pig Model of Myocardial Infarction: Assessment of Cell Survival, Engraftment, and Distribution by Hybrid Single Photon Emission Computed Tomography/Computed Tomography of Sodium Iodide Symporter Transgene Expression. Circulation *126*, 430–439.

Thomas, E.D. (1999). A history of haemopoietic cell transplantation. Br. J. Haematol. *105*, 330–339.

Toyota, T., Ohguri, N., Maruyama, K., Fujinami, M., Saga, T., and Aoki, I. (2012). Giant Vesicles Containing Superparamagnetic Iron Oxide as Biodegradable Cell-Tracking MRI Probes. Anal. Chem. *84*, 3952–3957.

Vasa, M., Fichtlscherer, S., Adler, K., Aicher, A., Martin, H., Zeiher, A.M., and Dimmeler, S. (2001). Increase in circulating endothelial progenitor cells by statin therapy in patients with stable coronary artery disease. Circulation *103*, 2885–2890.

Velde, G.V., Himmelreich, U., and Neeman, M. (2013). Reporter gene approaches for mapping cell fate decisions by MRI: promises and pitfalls. Contrast Media Mol. Imaging *8*, 424–431.

Vetter, A., Reinisch, A., Strunk, D., Kremser, C., Hahn, H.W., Huck, C.W., Ostermann, T., Leithner, K., and Bernkop-Schnürch, A. (2011). Thiolated polyacrylic acid-modified iron oxide nanoparticles for in vitro labeling and MRI of stem cells. J. Drug Target. *19*, 562–572.

Vinogradov, E., Soesbe, T.C., Balschi, J.A., Dean Sherry, A., and Lenkinski, R.E. (2012). pCEST: Positive contrast using Chemical Exchange Saturation Transfer. J. Magn. Reson. *215*, 64–73.

Yang, C., Rait, A., Pirollo, K.F., Dagata, J.A., Farkas, N., and Chang, E.H. (2008). Nanoimmunoliposome delivery of superparamagnetic iron oxide markedly enhances targeting and uptake in human cancer cells in vitro and in vivo. Nanomedicine Nanotechnol. Biol. Med. *4*, 318–329.

Yang, C.-Y., Hsiao, J.-K., Tai, M.-F., Chen, S.-T., Cheng, H.-Y., Wang, J.-L., and Liu, H.-M. (2010). Direct Labeling of hMSC with SPIO: the Long-Term Influence on Toxicity, Chondrogenic Differentiation Capacity, and Intracellular Distribution. Mol. Imaging Biol. *13*, 443–451.

Yoder, M.C., Mead, L.E., Prater, D., Krier, T.R., Mroueh, K.N., Li, F., Krasich, R., Temm, C.J., Prchal, J.T., and Ingram, D.A. (2007). Redefining endothelial progenitor cells via clonal analysis and hematopoietic stem/progenitor cell principals. Blood *109*, 1801–1809.